



A methodology to retrieve self-consistent aerosol optical properties using common aircraft measurements

Brian I. Magi,¹ Qiang Fu,¹ and Jens Redemann²

Received 4 December 2006; revised 13 March 2007; accepted 11 May 2007; published 23 October 2007.

[1] Aerosol optical properties that include the extinction coefficient, single scattering albedo, and asymmetry factor are needed to calculate the radiative effects of aerosols. However, measurements of these properties are typically limited to a few wavelengths, and direct measurements of the asymmetry factor are not available. We describe and evaluate a retrieval methodology that uses commonly collected aircraft-based measurements to derive self-consistent aerosol optical properties for the majority of the solar spectrum. Measurements of aerosol scattering and absorption at three wavelengths are required to constrain this retrieval. We apply the retrieval to vertical profiles of biomass burning aerosol data collected by the University of Washington (UW) research aircraft during the Southern African Regional Science Initiative field campaign (SAFARI-2000) and show that the retrieved (or “optically equivalent”) size distributions and wavelength-dependent refractive indices reproduce available aerosol optical measurements within their respective uncertainties. The retrieved optically equivalent size distribution characteristics are consistent with past studies, but the wavelength-dependent refractive indices retrieved using methods presented in this study are $\sim 14\%$ ($\sim 50\%$) greater than the real (imaginary) refractive indices retrieved from the Aerosol Robotic Network (AERONET) for three cases that were spatially and temporally colocated with the UW research aircraft. The retrieval presented in this study translates measured aerosol optical properties to parameters used directly as input to models and can be applied to any study that uses similar instrumentation. Provided that uncertainties are properly accounted for, self-consistent aerosol optical properties derived from measurements strengthen the unique contribution of in situ data collection to the modeling community.

Citation: Magi, B. I., Q. Fu, and J. Redemann (2007), A methodology to retrieve self-consistent aerosol optical properties using common aircraft measurements, *J. Geophys. Res.*, 112, D24S12, doi:10.1029/2006JD008312.

1. Introduction

[2] Aerosol optical properties are dependent on the aerosol chemical composition [Jacobson, 2001; Chung and Seinfeld, 2005], the chemical mixing state [Ackerman and Toon, 1981; Chylek et al., 1988], and the physical size distribution [Seinfeld and Pandis, 1998]. These fundamental properties are, however, difficult to fully characterize since aerosol lifetimes are short and the sources are heterogeneous [Bond et al., 2004; Reddy et al., 2005]. The uncertainty of radiative forcing due to aerosols is considered to be the largest source of uncertainty when estimating the sensitivity of climate to an increase in carbon dioxide [Anderson et al., 2003; Schwartz, 2004; Delworth et al., 2005; Hansen et al., 2005] and thus aerosols hinder precise predictions of the future climate [Andreae et al., 2005]. A number of field campaigns designed to characterize aerosol properties in different locations around the world have helped address the

uncertainties [Reid et al., 1998; Clarke et al., 2002; Russell et al., 2002; Swap et al., 2003; Doherty et al., 2005; Magi et al., 2005; Quinn and Bates, 2005; Redemann et al., 2006; Schmid et al., 2006].

[3] We describe a new methodology to retrieve aerosol optical properties from look-up tables of precalculated aerosol optical properties constructed using Mie theory [Bohren and Huffman, 1983; Seinfeld and Pandis, 1998; Ackerman and Toon, 1981]. Mie look-up tables can be used to determine the optical properties of an aerosol composed of spherical particles given the aerosol size distribution and complex refractive index. This is a “forward” calculation in the sense that the dependent variables, or the aerosol optical properties, are determined from the aerosol physical and chemical properties (or the independent variables).

[4] Alternatively, as discussed by Hartley [2000], Mie look-up tables can also be used to find an aerosol size distribution and complex refractive index that together produce specific aerosol optical properties. This is the “inverse” problem, where we find the independent variables using the dependent variables, and the solution to the inverse problem may not be unique [Redemann et al., 2000]. In this analysis, similar to the work of Redemann et al. [2000] and Hartley and Hobbs [2001], we present a method to solve the inverse

¹Department of Atmospheric Sciences, University of Washington, Seattle, Washington, USA.

²Bay Area Environmental Research Institute, Sonoma, California, USA.

problem and find the so-called optically equivalent aerosol size distribution and complex refractive index that together most closely reproduce available optical measurements. In contrast to those studies, however, we solve the inverse problem at multiple wavelengths.

[5] The goal of this study is to use commonly measured aerosol optical properties for a limited wavelength range, including the extinction coefficient and single scattering albedo, to derive self-consistent aerosol optical properties for a broader wavelength range. We apply the methodology to aircraft-based measurements collected during the Southern African Regional Science Initiative in August and September 2000 (SAFARI-2000) by the University of Washington (UW) research aircraft [Annegarn *et al.*, 2002; Swap *et al.*, 2003]. Descriptions and analyses of the UW aircraft data from SAFARI-2000 were discussed by Hobbs *et al.* [2003], Magi *et al.* [2003], Magi and Hobbs [2003], and Sinha *et al.* [2003]. B. I. Magi *et al.* (Using aircraft measurements to estimate the magnitude and uncertainty of the shortwave direct radiative forcing of southern African biomass burning aerosol, submitted to *Journal of Geophysical Research*, 2007, hereinafter referred to as Magi *et al.*, submitted manuscript, 2007) present a method to derive measurement-based estimates of southern African biomass burning aerosol radiative forcing using the methods in this study.

2. Methods

[6] In this section, we describe the technique used to find the best match between measured aerosol optical properties and aerosol optical properties calculated using Mie theory, which assumes that the particles are spherical. We model the aerosol size distribution with a unimodal lognormal function [e.g., Seinfeld and Pandis, 1998] which is a function of the geometric mean diameter (D_g), geometric standard deviation (σ_g), and the aerosol number concentration (N_a) for a specific range of particle diameters. The wavelength-dependent bulk aerosol complex refractive index ($m_\lambda = m_{r,\lambda} - im_{i,\lambda}$) describes how incident radiation with a wavelength λ interacts with the aerosol described by the unimodal lognormal size distribution.

[7] Extensive aerosol optical properties, or properties that are dependent on N_a , are the wavelength-dependent extinction ($\sigma_{\text{ext},\lambda}$), scattering ($\sigma_{\text{sca},\lambda}$), absorption ($\sigma_{\text{abs},\lambda}$), and backscattering ($\sigma_{\text{back},\lambda}$) coefficients. Values of $\sigma_{\text{ext},\lambda}$ can be determined by adding $\sigma_{\text{sca},\lambda}$ and $\sigma_{\text{abs},\lambda}$ and the wavelength-dependent aerosol optical depth (τ_λ) can be calculated by integrating $\sigma_{\text{ext},\lambda}$ over some vertical limits [e.g., Hartley and Hobbs, 2001; Magi *et al.*, 2003]. Intensive properties, or properties that are not dependent on N_a , are the wavelength-dependent single scattering albedo ($\omega_{o,\lambda}$), backscatter ratio (β_λ), and asymmetry parameter (g_λ). In all cases, the “ λ ” subscript notation indicates the dependence of the particular metric on wavelength, λ . The wavelength dependence of $\sigma_{\text{ext},\lambda}$, $\sigma_{\text{sca},\lambda}$, and $\sigma_{\text{abs},\lambda}$ are often given by the respective Angstrom exponents ($\alpha_{\text{ext},\lambda}$, $\alpha_{\text{sca},\lambda}$, and $\alpha_{\text{abs},\lambda}$) which are defined as the slopes of the optical properties with respect to wavelength on logarithmic scale. All aerosol optical properties discussed in this study are defined by Seinfeld and Pandis [1998] and a number of other widely available sources.

2.1. Description of Look-Up Tables

[8] We store aerosol optical properties calculated using Mie theory in multidimensional look-up tables. The input ($\mathbf{M}_{\text{input}}$) to a well-documented, publicly available Mie scattering code [Dave, 1970; Wiscombe, 1980; ftp://climate1.gsfc.nasa.gov/wiscombe/] is defined as

$$\mathbf{M}_{\text{input}} = [\lambda, m_r, m_i, D_g, \sigma_g, N_a] \quad (1)$$

where the terms are discussed in section 2. The basic output of the Mie scattering code gives the extinction, scattering, and backscattering efficiency factors at a wavelength λ ($Q_{\text{ext},\lambda}$, $Q_{\text{sca},\lambda}$, and $Q_{\text{back},\lambda}$, respectively) for a single spherical particle of diameter D_p with a particular refractive index. As described by Bohren and Huffman [1983], we can then integrate $Q_{\text{ext},\lambda}$, $Q_{\text{sca},\lambda}$, and $Q_{\text{back},\lambda}$ over a range of D_p for the lognormal size distribution given by D_g , σ_g , and N_a in $\mathbf{M}_{\text{input}}$ to arrive at the size-integrated optical properties in the output matrix ($\mathbf{M}_{\text{output}}$) defined as

$$\mathbf{M}_{\text{output}} = [\sigma_{\text{ext},\lambda}, \omega_{o,\lambda}, \beta_\lambda, g_\lambda] \quad (2)$$

where the elements of $\mathbf{M}_{\text{output}}$ are defined in section 2 and below. We integrate from $D_{p,\text{min}} = 0.01 \mu\text{m}$ to $D_{p,\text{max}} = 10 \mu\text{m}$ to calculate

$$\sigma_{x,\lambda} = \int_{D_{p,\text{min}}}^{D_{p,\text{max}}} \frac{\pi D^2}{4} Q_{x,\lambda}(D) n(D) dD \quad (3)$$

where the “ x ” subscript can mean “ext,” “sca,” or “back” such that we can calculate $\sigma_{\text{ext},\lambda}$, $\sigma_{\text{sca},\lambda}$, or $\sigma_{\text{back},\lambda}$, respectively, given the appropriate efficiency factor, and $n(D)$ is specified by the lognormal function defined by D_g , σ_g , and N_a in $\mathbf{M}_{\text{input}}$ [e.g., Seinfeld and Pandis, 1998]. Using equation (3), we can calculate $\omega_{o,\lambda} = \sigma_{\text{sca},\lambda}/\sigma_{\text{ext},\lambda}$ and $\beta_\lambda = \sigma_{\text{back},\lambda}/\sigma_{\text{sca},\lambda}$. We then calculate the asymmetry parameter (g_λ) as

$$g_\lambda = \frac{\int_{D_{p,\text{min}}}^{D_{p,\text{max}}} g_\lambda(D) \frac{\pi D^2}{4} Q_{\text{sca},\lambda}(D) n(D) dD}{\sigma_{\text{sca},\lambda}} \quad (4)$$

where again we integrate the lognormal function from $D_{p,\text{min}} = 0.01 \mu\text{m}$ to $D_{p,\text{max}} = 10 \mu\text{m}$.

[9] The ranges of the elements of $\mathbf{M}_{\text{input}}$ are listed in Table 1. Although N_a for real aerosols varies, the elements of $\mathbf{M}_{\text{output}}$ are calculated using $N_a = 1000 \text{ cm}^{-3}$. Extensive properties can be rescaled to other values of N_a as necessary. This saves computation time and significantly reduces the size of $\mathbf{M}_{\text{output}}$.

[10] The ranges of the five remaining dimensions of $\mathbf{M}_{\text{input}}$ are larger. The wavelength dimension is set to 15 wavelengths between $\lambda = 354$ and 1557 nm , for reasons that we discuss in section 3.1. Each wavelength dimension is treated as a separate look-up table in the sense that we specifically calculate optical properties at each of the 15 wavelengths for the same range of sizes.

[11] There are 12 values of m_r between 1.4 and 1.95, and 26 values of m_i between 0 and 0.6 in $\mathbf{M}_{\text{input}}$. The ranges are based on information published by d’Almeida *et al.* [1991]

Table 1. Ranges of the Input ($\mathbf{M}_{\text{input}}$ in Equation (1)) Used to Build the Aerosol Optical Properties Look-Up Tables^a

Parameter	Range	Step Size	Number of Values
λ , nm	354, 380, 449, 450 , 499, 525, 550 , 606, 675, 700 , 778, 865, 1019, 1241, 1557	variable	15
m_r	1.4–1.95	0.05	12
m_i	0–0.1, 0.1–0.6	0.005, 0.1	26
D_g , μm	0.06–0.985	0.025	38
σ_g	1.1–3.1	0.05	41
N_a , cm^{-3}	1000	N/A	1

^aThis includes the individual wavelengths (λ), the real and imaginary parts of the refractive index (m_r and m_i , respectively), the geometric mean diameter (D_g), geometric standard deviation (σ_g), and the aerosol number concentration (N_a), with units (if applicable) listed in the table. Bold values of λ indicate in situ measurement wavelengths, while the remaining values of λ correspond to the Sun photometer.

and cover complex refractive indices ranging from water with inclusions to pure soot particles. The lower limit of m_r is set at 1.4 because the low ambient relative humidity during SAFARI-2000 [Magi *et al.*, 2003] suggests a small contribution of condensed water to the aerosol composition and therefore it is unlikely that the SAFARI-2000 aerosol bulk refractive index would approach that of pure water ($m_{r,\text{water}} = 1.33$). For more general application, values of m_r less than 1.4 should be used. The upper limits of m_r and m_i are those listed by *d'Almeida et al.* [1991] for a pure soot particle. However, except in areas close to combustion sources (urban highway, near a cookstove), an aerosol is unlikely to be entirely composed of soot particles [Kirchstetter *et al.*, 2004; Bond and Bergstrom, 2006; Roden *et al.*, 2006].

[12] We use 38 evenly spaced values of D_g from 0.06 to 0.985 μm with intervals of 0.025 μm and 41 evenly spaced values of σ_g from 1.1 to 3.1 with intervals of 0.1 in $\mathbf{M}_{\text{input}}$. Limiting D_g to values less than 1 μm implies that we are assuming the aerosol size distribution is dominated by submicron particles. Since σ_g determines the width of the

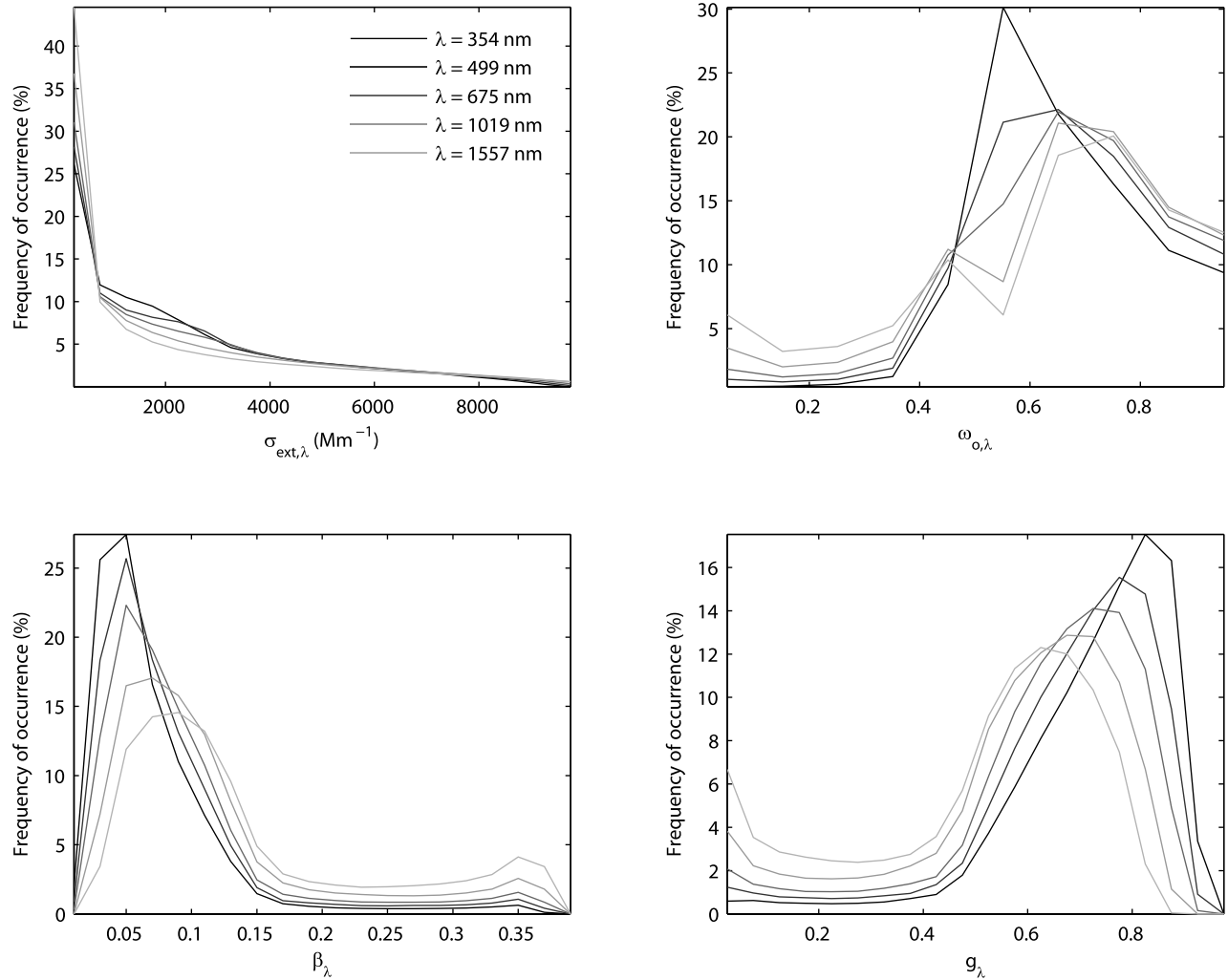


Figure 1. Frequency of occurrence (%) in the look-up tables of the wavelength-dependent extinction coefficient ($\sigma_{\text{ext},\lambda}$) using $N_a = 1000 \text{ cm}^{-3}$, single scattering albedo ($\omega_{o,\lambda}$), backscatter ratio (β_λ), and asymmetry parameter (g_λ) calculated from the input to the Mie calculations listed in Table 1. The total number of possible values for each optical property at each wavelength (λ) is 486,096. Five of the fifteen wavelengths are shown in each of the figures.

size distribution, the range of σ_g in $\mathbf{M}_{\text{input}}$ implies size distributions that extend beyond 1 μm diameter (for example, if $D_g = 0.985 \mu\text{m}$ and $\sigma_g = 3.1$). Magi [2006] used measurements to estimate the aerosol coarse mode volume fraction as the coarse mode (particles with diameters of $\sim 1\text{--}3 \mu\text{m}$) particle volume divided by fine mode (particles with diameters of $\sim 0.1\text{--}1 \mu\text{m}$) particle volume and found that during SAFARI-2000, the average coarse mode volume fraction was $(3 \pm 2)\%$, which is consistent with general biomass burning particle sizes [Reid et al., 2005a, 2005b].

[13] The distribution of the calculated optical properties in $\mathbf{M}_{\text{output}}$ for five of the 15 wavelengths and the full range of the remaining dimensions of $\mathbf{M}_{\text{input}}$ (Table 1) are shown in Figure 1. Each element of $\mathbf{M}_{\text{output}}$ (i.e., $\sigma_{\text{ext},\lambda}$, $\omega_{o,\lambda}$, β_λ , and g_λ) will have $12 \times 26 \times 38 \times 41 = 486,096$ possible values for each of the 15 wavelengths. The distribution of $\omega_{o,\lambda}$ shown in Figure 1 has a noticeable dip between about 0.45 and 0.6 that arises from the discontinuity in the resolution of the m_i dimension of $\mathbf{M}_{\text{input}}$ where, for $m_i > 0.1$, we decrease the resolution from 0.005 to 0.1. The decrease in resolution should not affect retrievals of biomass burning aerosol optical properties since biomass burning particles age rapidly away from the source [Magi and Hobbs, 2003] and values of $m_i > 0.1$ are generally thought to only occur close to combustion sources [Bond and Bergstrom, 2006; Roden et al., 2006]. Adjacent values of the individual elements of $\mathbf{M}_{\text{output}}$ are separated by very small numbers relative to the magnitudes of values, which suggests a nearly continuous spectrum of values. For example, 99% of the values of $\omega_{o,\lambda}$ in the look-up tables are separated by less than 0.000027. The look-up tables were designed to be able to resolve optical properties ($\mathbf{M}_{\text{output}}$) within typical uncertainties that arise from instrument noise, natural variability, and measurement correction factors [Magi et al., 2003] (also section 3.1).

2.2. Retrieval of Optically Equivalent Properties

[14] The first part of the retrieval finds the optically equivalent unimodal lognormal submicron size distribution (described by $D_{g,\text{oe}}$, $\sigma_{g,\text{oe}}$, and $N_{a,\text{oe}}$) and the optically equivalent refractive indices ($m_{\text{oe},\lambda}$) at $\lambda = 450, 550$, and 700 nm that together most closely reproduce measured values of $\sigma_{\text{ext},\lambda}$, $\omega_{o,\lambda}$, and β_λ at $\lambda = 450, 550$, and 700 nm . The measurement matrix is defined as

$$\Psi_{\text{meas},\lambda,z} = [\sigma_{\text{ext,meas},\lambda,z}, \omega_{o,\text{meas},\lambda,z}, \beta_{\text{meas},\lambda,z}] \quad (5)$$

where the “ λ ” and “ z ” subscripts indicate the dependence of the measurements on wavelength and altitude, respectively. Similarly, the uncertainty matrix is defined as

$$\delta_{\text{meas},\lambda,z} = [\delta\sigma_{\text{ext,meas},\lambda,z}, \delta\omega_{o,\text{meas},\lambda,z}, \delta\beta_{\text{meas},\lambda,z}] \quad (6)$$

where each element of $\delta_{\text{meas},\lambda,z}$ is the uncertainty associated with the corresponding element of $\Psi_{\text{meas},\lambda,z}$ and is derived from measurement uncertainty and natural variability (section 3.1). The matrix of calculated values from the look-up tables are defined as

$$\Psi_{\text{calc},\lambda,z} = [\sigma_{\text{ext,calc},\lambda,z}, \omega_{o,\text{calc},\lambda,z}, \beta_{\text{calc},\lambda,z}] \quad (7)$$

To solve the inverse problem, we calculate

$$\chi_{\lambda,z}^2 = \sum_{j=1}^3 \left[\frac{\Psi_{\text{meas},\lambda,z}^j - \Psi_{\text{calc},\lambda,z}^j}{\delta_{\text{meas},\lambda,z}^j} \right]^2 \quad (8)$$

for each wavelength (λ) and at each altitude (z), where $\Psi_{\text{meas},\lambda,z}^{j=1} = \sigma_{\text{ext,meas},\lambda,z}$, $\Psi_{\text{meas},\lambda,z}^{j=2} = \omega_{o,\text{meas},\lambda,z}$, and $\Psi_{\text{meas},\lambda,z}^{j=3} = \beta_{\text{meas},\lambda,z}$, with analogous definitions for $\Psi_{\text{calc},\lambda,z}^j$ and $\delta_{\text{meas},\lambda,z}^j$. To reduce computations, we calculate $\chi_{\lambda,z}^2$ only when $(\Psi_{\text{meas},\lambda,z}^j - \Psi_{\text{calc},\lambda,z}^j)^2 < (\delta_{\text{meas},\lambda,z}^j)^2$. All values of $\chi_{\lambda,z}^2$ are found for each wavelength.

[15] To further reduce computations, we require the number of possible solutions for each wavelength to be between 20 and 100 by allowing $\delta_{\text{meas},\lambda,z}$ to be flexible. If more than 100 solutions are found at a particular wavelength, we reduce $\delta_{\text{meas},\lambda,z}$ by 5% until less than 100 solutions are found. Similarly, we increase $\delta_{\text{meas},\lambda,z}$ by 10–50% if the number of solutions is less than 20.

[16] We now have a set of possible solutions at each wavelength. The optically equivalent size distribution and refractive indices are defined as

$$\phi_{\text{oe},\lambda,z} = [m_{r,\text{oe},\lambda,z}, m_{i,\text{oe},\lambda,z}, D_{g,\text{oe},z}, \sigma_{g,\text{oe},z}, N_{a,\text{oe},z}] \quad (9)$$

and are determined by searching every combination of the solutions at all the wavelengths for a single size distribution that both minimizes the values of $\chi_{\lambda,z}^2$ and minimizes the differences in the size distribution parameters across the three wavelengths. Values of the wavelength-dependent optically equivalent asymmetry parameter ($g_{\text{oe},\lambda}$) are subsequently determined by Mie theory calculations using the parameters in $\phi_{\text{oe},\lambda,z}$.

[17] To retrieve $\phi_{\text{oe},\lambda,z}$ at a particular wavelength and altitude, we constrain the search with the three parameters specified by $\Psi_{\text{meas},\lambda,z}$ and the corresponding uncertainties in $\delta_{\text{meas},\lambda,z}$. The number of parameters retrieved in $\phi_{\text{oe},\lambda,z}$ at a particular wavelength and altitude is five. Thus a one wavelength retrieval is an underdetermined problem (three knowns, five unknowns). However, if we run the retrieval for data at three wavelengths, we have nine known values and nine unknown values since we are searching for a single size distribution (described by three parameters) and a wavelength-dependent complex refractive index (two parameters for every wavelength). Therefore we need measured scattering, backscattering, and absorption properties at least at three wavelengths to derive the optically equivalent size distribution defined by $D_{g,\text{oe}}$, $\sigma_{g,\text{oe}}$, and $N_{a,\text{oe}}$. These parameters, along with the retrieved $m_{r,\text{oe},\lambda}$ and $m_{i,\text{oe},\lambda}$, can be used to derive the values of $g_{\text{oe},\lambda}$. The retrieved optically equivalent size distribution can then be used to constrain aerosol optical properties at other solar wavelengths.

2.3. Self-Consistent Aerosol Properties

[18] At other wavelengths where the extinction coefficient and single scattering albedo are available, we can use these information along with the optically equivalent size distribution obtained in section 2.2 to retrieve $m_{r,\text{oe}}$ and $m_{i,\text{oe}}$ at the other wavelengths. Thus the goal of the second part of the retrieval is to find self-consistent aerosol optical properties such that a size distribution and refractive index at a

particular wavelength can be combined to calculate optical properties relevant to radiative transfer calculations. This part of the retrieval accesses the look-up tables differently because we have different inputs to use as constraints. The new measurement matrix is defined as

$$\Psi_{\text{meas},\lambda,z} = [\sigma_{\text{ext,meas},\lambda,z}, \omega_{\text{o,meas},\lambda,z}, D_{\text{g,oe},z}, \sigma_{\text{g,oe},z}, N_{\text{a,oe},z}] \quad (10)$$

where $\sigma_{\text{ext,meas},\lambda,z}$ and $\omega_{\text{o,meas},\lambda,z}$ are measurements made at wavelengths where $\beta_{\text{meas},\lambda,z}$ is unavailable, and $D_{\text{g,oe},z}$, $\sigma_{\text{g,oe},z}$, and $N_{\text{a,oe},z}$ are from $\phi_{\text{oe},\lambda,z}$ in equation (9). The uncertainty matrix is defined as

$$\Delta_{\text{meas},\lambda,z} = [\delta\sigma_{\text{ext,meas},\lambda,z}, \delta\omega_{\text{o,meas},\lambda,z}, \delta D_{\text{g,oe},z}, \delta\sigma_{\text{g,oe},z}, \delta N_{\text{a,oe},z}] \quad (11)$$

where $\delta\sigma_{\text{ext,meas},\lambda,z}$ and $\delta\omega_{\text{o,meas},\lambda,z}$ are the uncertainty associated with $\sigma_{\text{ext,meas},\lambda,z}$ and $\omega_{\text{o,meas},\lambda,z}$ and $\delta D_{\text{g,oe},z}$, $\delta\sigma_{\text{g,oe},z}$, and $\delta N_{\text{a,oe},z}$ are determined from the range of values retrieved in $\phi_{\text{oe},\lambda,z}$. The matrix of calculated values from the look-up tables is defined as

$$\Psi_{\text{calc},\lambda,z} = [\sigma_{\text{ext,calc},\lambda,z}, \omega_{\text{o,calc},\lambda,z}, D_{\text{g,oe,calc},z}, N_{\text{a,oe,calc},z}] \quad (12)$$

To find self-consistent aerosol optical properties, we calculate

$$X_{\lambda,z}^2 = \sum_{j=1}^5 \left[\frac{\Psi_{\text{meas},\lambda,z}^j - \Psi_{\text{calc},\lambda,z}^j}{\Delta_{\text{meas},\lambda,z}^j} \right]^2 \quad (13)$$

where we sum the values of $X_{\lambda,z}^2$ for the five elements of $\Psi_{\text{meas},\lambda,z}$, $\Psi_{\text{calc},\lambda,z}$, and $\Delta_{\text{meas},\lambda,z}$. We retrieve the optically equivalent refractive indices as

$$\Phi_{\text{oe},\lambda,z} = [m_{\text{r,oe},\lambda,z}, m_{\text{i,oe},\lambda,z}] \quad (14)$$

by finding the minimum value of $X_{\lambda,z}^2$. The crucial part of finding self-consistent aerosol optical properties is the constraint on absorption given by values of $\omega_{\text{o,meas},\lambda,z}$ in equation (10). After evaluating uncertainties associated with the finite dimensions of the look-up tables in section 2.4, we apply the retrieval methodology in sections 2.2 and 2.3 to real data in section 3.

2.4. Structural Uncertainty

[19] The uncertainty that arises from the retrieval itself, or the structural uncertainty, is estimated by calculating aerosol optical properties from a predetermined size distribution and refractive index. However, instead of using one of the discrete values specific to the look-up table used in the retrieval, we calculate the optical properties from a value between the discrete steps used to build the look-up table. For example, referring to Table 1, we could calculate the optical properties at $\lambda = 550$ nm using $D_{\text{g}} = 0.1475 \mu\text{m}$, $\sigma_{\text{g}} = 1.7$, and $m_{550} = 1.60 - 0.02i$, noting that the value of D_{g} falls between the values in Table 1 (i.e., $D_{\text{g}} = 0.135$ and $0.160 \mu\text{m}$) used to build the look-up tables. Thus, although we have an exact solution using Mie theory, this particular exact solution is not explicitly in the look-up tables.

[20] We retrieve $\phi_{\text{oe},\lambda}$ using a range of predetermined values of D_{g} , σ_{g} , m_{r} , and m_{i} . We independently investigate the uncertainty that arises from each of the input values such that we begin by choosing values of D_{g} that are not explicitly used in look-up table calculations (per the example above) while simultaneously choosing values of σ_{g} , m_{r} , and m_{i} that are used in the look-up table calculations. We then choose values of σ_{g} not used in look-up table calculations while using values of D_{g} , m_{r} , and m_{i} that are used in the look-up table calculations. The same procedure is repeated for m_{r} , followed by m_{i} . The average percent difference between the exact solution and the calculated optical properties for each dimension of $\mathbf{M}_{\text{input}}$ is the error associated with that particular dimension of $\mathbf{M}_{\text{input}}$. These average percent differences are propagated together by quadratures for each of the calculated aerosol optical properties. Using this method, we calculate $\pm 4.1\%$ uncertainty in $\sigma_{\text{ext},\lambda}$, $\pm 1.2\%$ in $\omega_{\text{o},\lambda}$, and $\pm 3.8\%$ in g_{λ} , keeping in mind that these so-called structural uncertainties are entirely an artifact of the retrieval and apply only to the calculated (or retrieved) aerosol optical properties. It is important to note that these derived structural uncertainties must be propagated together with the measurement uncertainties used in equations (6) and (10) and that we discuss in sections 3.1 and 3.2 and in Figure 5.

[21] Partitioning the structural uncertainty, we find that the smallest contribution to the structural uncertainty in all calculated optical properties arises from the values of D_{g} used to build the look-up table. The greatest contribution to the structural uncertainty arises from the values of m_{r} for $\sigma_{\text{ext},\lambda}$ and g_{λ} , but from m_{i} for $\omega_{\text{o},\lambda}$. Thus we can most efficiently reduce the structural uncertainties associated with the look-up tables used in the retrieval by increasing the resolution of the values of m_{r} and m_{i} used to build the look-up tables.

3. Application

3.1. Aircraft Data

[22] We apply the retrieval methodology to six vertical profiles of aircraft-based data collected during SAFARI-2000 and described by *Magi et al.* [2003] and *Magi* [2006]. The vertical profiles were collected on 22 August over Skukuza, South Africa, 24 August over Inhaca Island, Mozambique, 31 August in southern Mozambique, 3 September over Sua Pan, Botswana, and two profiles were obtained near Mongu, Zambia on 6 September (0917–0929 and 0957–1014 UTC), where all dates refer to the year 2000. The vertical resolution of the profiles was 150 m. The full suite of measurements has been described previously [*Magi et al.*, 2003; *Sinha et al.*, 2003; *Magi*, 2006], but we summarize the measurements most important to this study.

[23] We measured $\sigma_{\text{sca},\lambda}$ and β_{λ} at $\lambda = 450, 550,$ and 700 nm for $D_{\text{p}} < 2 \mu\text{m}$ using a 3λ -nephelometer custom built for the UW and similar in design to the commercially available TSI 3λ -nephelometer [*Magi et al.*, 2003]. All data from the 3λ -nephelometer were corrected according to protocols described by *Hartley* [2000], which are similar to those described by *Anderson et al.* [1996] and *Anderson and Ogren* [1998] for the TSI nephelometer. The values of $\sigma_{\text{sca},\lambda}$ and β_{λ} are adjusted to ambient relative humidity (RH) based on the work of *Magi and Hobbs* [2003], although the

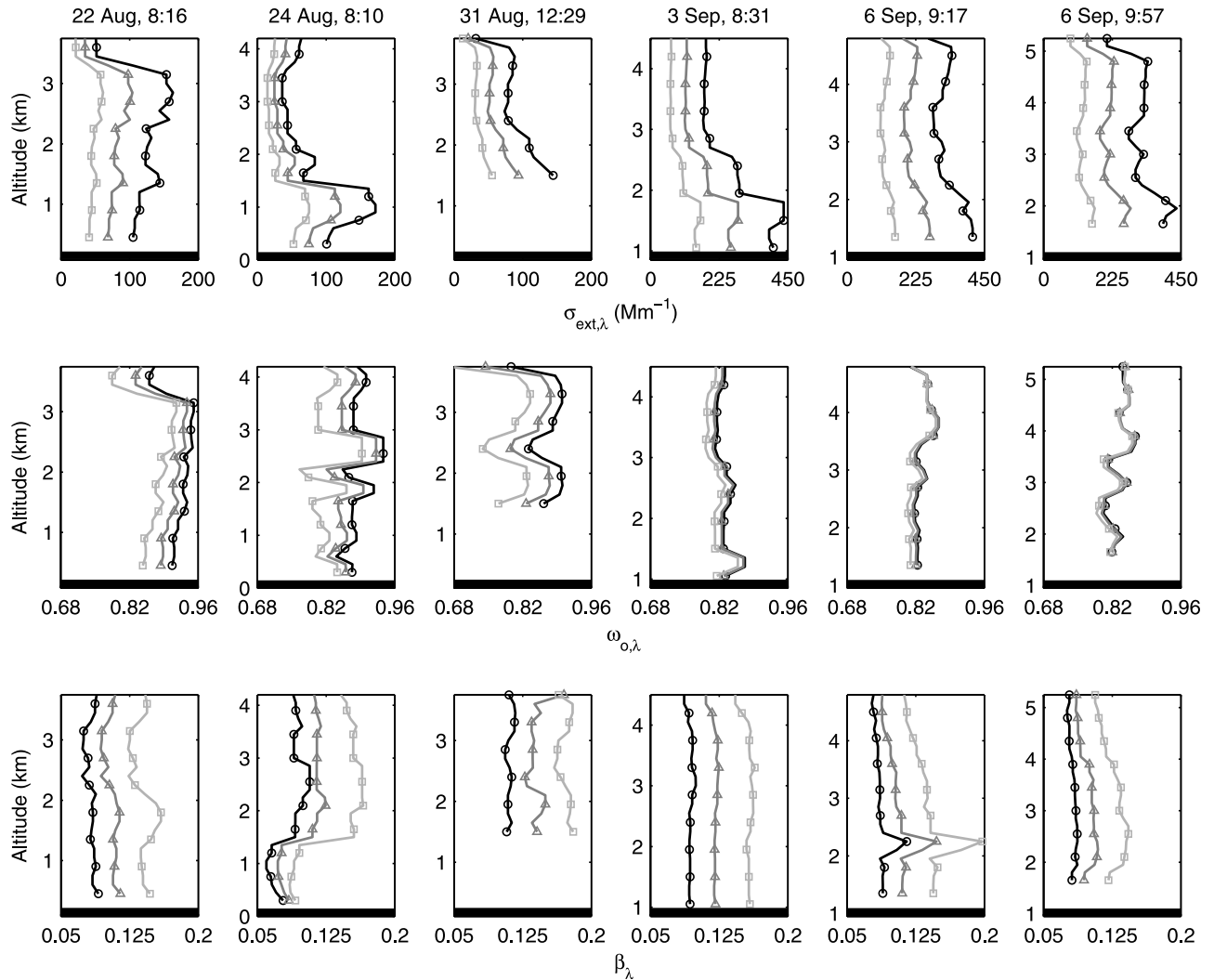


Figure 2. Vertical profiles of the wavelength-dependent (λ) extinction coefficient ($\sigma_{\text{ext},\lambda}$), single scattering albedo ($\omega_{o,\lambda}$), and backscatter ratio (β_{λ}) obtained during SAFARI-2000 by the UW research aircraft. The titles of each of the six columns refer to the date (year 2000) and UTC time of the vertical profiles (as listed in Table 2). The solid lines with circles, shaded lines with triangles, and light shaded lines with squares correspond to $\lambda = 450, 550$ and 700 nm, respectively. The thick horizontal solid line is the surface, and the altitudes are above mean sea level. The scales on the x axes are the same for $\omega_{o,\lambda}$ and β_{λ} , but more than a factor of two larger for the vertical profiles of $\sigma_{\text{ext},\lambda}$ collected in September 2000.

corrections are small since ambient RH during SAFARI-2000 was usually less than 50% [Magi *et al.*, 2003]. The 3λ -nephelometer was calibrated before and during SAFARI-2000 by standard procedures described by Anderson and Ogren [1998], but Anderson *et al.* [1996, 2000] show that TSI nephelometer measurements have a $\pm 7\%$ systematic uncertainty that cannot be averaged out. We assume that this systematic uncertainty applies to the 3λ -nephelometer used in SAFARI-2000. All uncertainties (systematic uncertainty, natural variability, instrument noise, and correction factor uncertainty) are propagated using standard quadratures methods [Bevington and Robinson, 1992].

[24] We measured $\sigma_{\text{abs},550}$ for $D_p < 2 \mu\text{m}$ with a commercially available particle and soot absorption photometer (PSAP) and corrected the PSAP output according to protocols described by Bond *et al.* [1999], who also show that there is $\pm 20\%$ systematic uncertainty associated with the PSAP

measurements. Part of the correction procedure described by Bond *et al.* [1999] is to verify the flow rates in the PSAP, but because we were unable to quantitatively confirm the flow rates of the specific PSAP used during SAFARI-2000, we assume a slightly higher systematic uncertainty of $\pm 25\%$. We extrapolate $\sigma_{\text{abs},550}$ to $\sigma_{\text{abs},450}$ and $\sigma_{\text{abs},700}$ using an assumed value of the absorption angstrom exponent (α_{abs}). The value of α_{abs} varies as a function of the aerosol source, composition, and age [Kirchstetter *et al.*, 2004; Ganguly *et al.*, 2005; Bond and Bergstrom, 2006; Roden *et al.*, 2006], but we assume that for the aged biomass burning aerosol in the regional haze of southern Africa, $\alpha_{\text{abs}} = 1$ for August vertical profiles and $\alpha_{\text{abs}} = 2$ for September vertical profiles, based on an analysis of SAFARI-2000 data by Bergstrom *et al.* [2003]. We propagate an additional $\pm 10\%$ and $\pm 12\%$ systematic uncertainty for values of $\sigma_{\text{abs},450}$ and $\sigma_{\text{abs},700}$ due to the uncertainty associated with the assumed value of α_{abs} . The

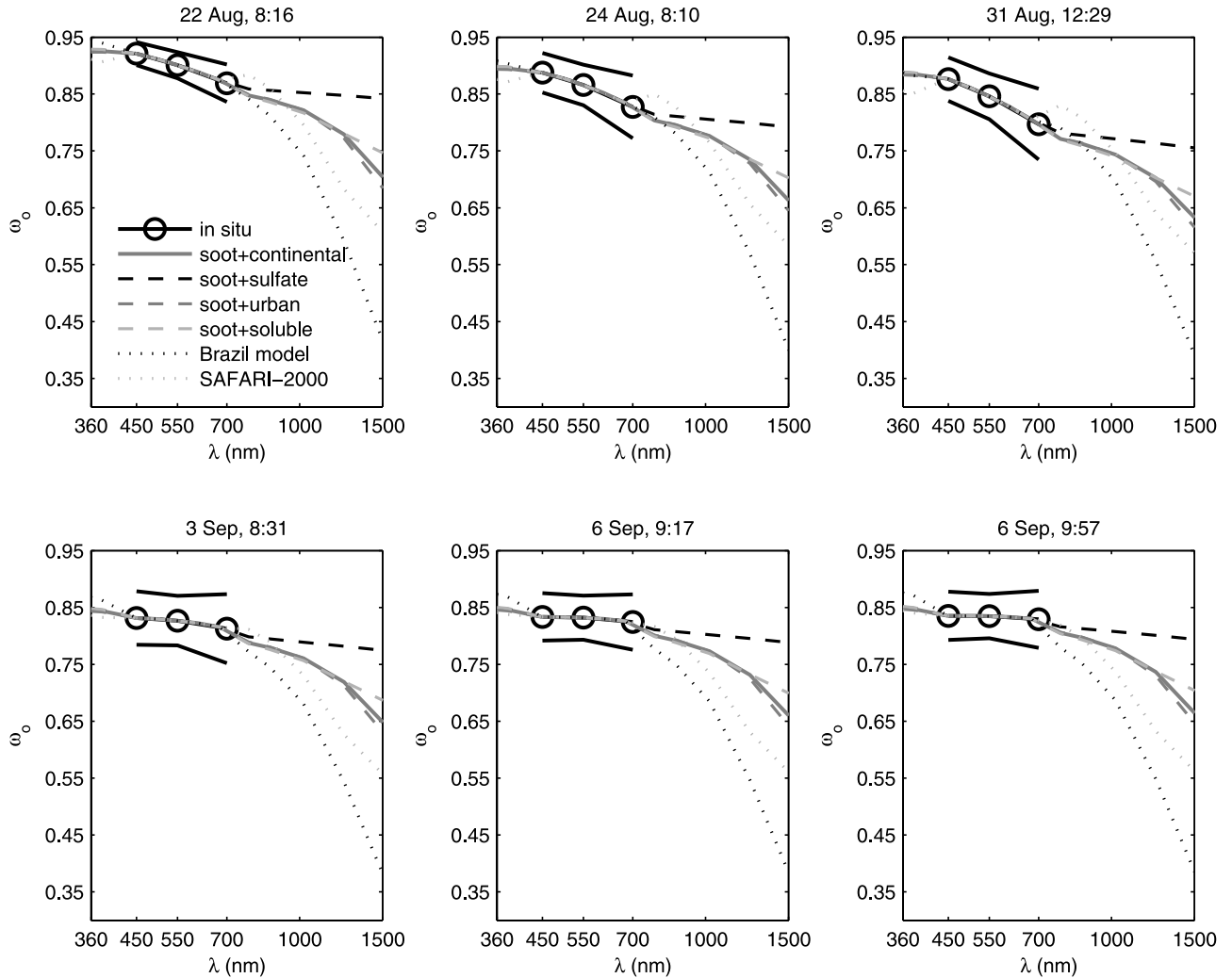


Figure 3. Different possible constraints on single scattering albedo (ω_0) as a function of wavelength (λ) for the six UW research aircraft vertical profiles, noting that the titles refer to the date (year 2000) and UTC times listed in Table 2. Referring to the legend, “in situ” is ω_0 derived from the nephelometer and particle and soot absorption photometer data at $\lambda = 450, 550,$ and 700 nm, whereas the “soot” combinations refer to different generic aerosol types given by *d’Almeida et al.* [1991]. The thick shaded line for “soot + continental” is the aerosol combination that we use to constrain $\omega_{0,\lambda}$ in this study for nonvisible wavelengths. The Brazil model is from *Ross et al.* [1998], and the SAFARI-2000 curve is from derived values of $\omega_{0,\lambda}$ for a case study described by *Bergstrom et al.* [2003].

values of $\pm 10\%$ and $\pm 12\%$ arise by assuming that half of the full range of the difference between extrapolating $\sigma_{\text{abs},550}$ to $\sigma_{\text{abs},450}$ and $\sigma_{\text{abs},700}$ using $\alpha_{\text{abs}} = 1$ and $\alpha_{\text{abs}} = 2$ is the uncertainty.

[25] By assuming α_{abs} for visible wavelength, we lose a constraint on the retrieval and are left with eight knowns and nine unknowns. We account for this by using data collected with a TSI, Inc. Condensation Nuclei Counters (CNC) that sampled from the same inlet as the 3λ -nephelometer and the PSAP on the UW research aircraft. The CNC (TSI model 3022) measures N_a for $D_p = 0.007\text{--}1\ \mu\text{m}$, which is nearly the same as the size range used to compile the look-up tables in the retrieval (Table 1). Thus we use N_a as an additional constraint on the retrieval and have nine knowns and eight unknowns.

[26] The second part of the retrieval uses data collected with the NASA Ames Airborne Tracking Sun photometer, which we simply call the Sun photometer [*Magi et al.*, 2003; *Schmid et al.*, 2003, 2006]. Under cloudless conditions, the Sun photometer reported the aerosol optical depth (τ_λ) above the altitude of the aircraft at 12 wavelengths during SAFARI-2000 [*Magi et al.*, 2003; *Schmid et al.*, 2003]. Values of $\sigma_{\text{ext},\lambda}$ can be derived by differentiating τ_λ at two vertically separated points, but uncertainties in these derived values are $\sim 15\text{--}20\%$ [*Schmid et al.* 2003, 2006]. *Magi et al.* [2003] showed that τ_{550} derived from the 3λ -nephelometer and the PSAP compared to within 0.04 or 13% (root mean squared difference) with the Sun photometer measurements of τ_{550} , and that the in situ derived τ_{550} are biased low by 2%, on average, suggesting that the submicron particles dominated the optical properties.

Table 2. Information About the Six Vertical Profiles Used in the Retrieval as Well as the Column-Averaged, Extinction-Weighted Mean Values of the Geometric Mean Diameter (D_g), Geometric Standard Deviation (σ_g), and Submicron Diameter Aerosol Number Concentration (N_a) of the Lognormal Optically Equivalent Size Distribution^a

ID	Date (2000)	Latitude, °S	Longitude, °E	UTC Time, hhmm	Altitude, km	Surface Elevation, km	Optically Equivalent Size Distribution Parameters			
							D_g , μm	σ_g	N_a , cm^{-3}	
1	22 Aug	24.98 ± 0.04	31.61 ± 0.06	0816–1006	0.37–3.82	0.15	0.173 ± 0.007	1.886 ± 0.085	2438 ± 59	
2	24 Aug	25.98 ± 0.03	32.91 ± 0.02	0810–0824	0.21–4.12	0.07	0.196 ± 0.025	1.923 ± 0.218	1508 ± 217	
3	31 Aug	21.62 ± 0.17	34.27 ± 0.13	1229–1244	0.64–3.89	0.19	0.152 ± 0.013	1.732 ± 0.062	4600 ± 48	
4	3 Sep	20.59 ± 0.03	26.17 ± 0.02	0831–0850	1.08–4.58	0.93	0.215 ± 0.011	1.674 ± 0.059	4291 ± 70	
5	6 Sep	15.19 ± 0.05	23.16 ± 0.03	0917–0929	1.37–4.77	1.03	0.198 ± 0.007	1.799 ± 0.062	4430 ± 102	
6	6 Sep	15.47 ± 0.22	23.46 ± 0.16	0957–1014	1.64–5.27	1.03	0.189 ± 0.006	1.854 ± 0.058	4279 ± 117	
Average ± standard deviation								0.187 ± 0.022	1.811 ± 0.095	3591 ± 1292

^aThe vertical profiles can also be cross-referenced with information in Table 3 using the numerical identification (ID).

[27] The six vertical profiles of $\sigma_{\text{ext},\lambda,z}$, $\omega_{o,\lambda,z}$, and $\beta_{\lambda,z}$ at $\lambda = 450, 550,$ and 700 nm and varying altitude (z) ranges are shown in Figure 2. The values of $\sigma_{\text{ext},\lambda,z}$ are calculated as the sum of $\sigma_{\text{sca},\lambda,z}$ and $\sigma_{\text{abs},\lambda,z}$, but are adjusted to match values of $\sigma_{\text{ext},\lambda,z}$ derived from the Sun photometer. The adjustment for SAFARI-2000 was generally ~ 15 – 30% and is consistent with the thinking that in situ measurements are typically biased low with respect to the Sun photometer [Schmid et al., 2006]. The values of $\omega_{o,\lambda,z}$ are calculated as $\sigma_{\text{sca},\lambda,z}/(\sigma_{\text{sca},\lambda,z} + \sigma_{\text{abs},\lambda,z})$. More details about the profiles can be found in the works of Magi et al. [2003], Leahy et al. [2007], and Magi [2006].

3.2. Retrieval Using Aircraft Data

[28] From the available measurements at $\lambda = 450, 550,$ and 700 nm shown in Figure 2, we specify $\psi_{\text{meas},\lambda,z}$ (equation (5)), while $\delta_{\text{meas},\lambda,z}$ (equation (6)) is determined by the uncertainties associated with each instrument. Using look-up tables at $\lambda = 450, 550,$ and 700 nm, we retrieve $\phi_{\text{oe},\lambda,z}$ in equation (9).

[29] Values of $\sigma_{\text{ext},\text{meas},\lambda,z}$ derived from the Sun photometer at 12 wavelengths between 354 and 1557 nm and the optically equivalent size distribution ($\phi_{\text{oe},\lambda,z}$) found by using information at $\lambda = 450, 550,$ and 700 nm make up part of $\Psi_{\text{meas},\lambda,z}$ in equation (10). Aside from $\omega_{o,550,z}$, however, direct measurements of $\omega_{o,\lambda,z}$ from SAFARI-2000 do not exist. As explained above, we can justifiably extrapolate $\sigma_{\text{abs},550,z}$ to other visible wavelengths using suggested values for α_{abs} from Bergstrom et al. [2003], but the extrapolation does not necessarily apply to nonvisible wavelengths such as the near infrared (NIR) or ultraviolet (UV) wavelength regions. This deficiency in the understanding of the wavelength dependence of absorption (i.e., α_{abs}) is not unique to SAFARI-2000 [Bond and Bergstrom, 2006].

[30] In lieu of measurements of $\omega_{o,\lambda,z}$ in the NIR and UV, we impose artificial constraints on $\omega_{o,\lambda,z}$ by linearly combining the soot and continental aerosol types in the d’Almeida et al. [1991] aerosol climatology (identical to models given by Hess et al. [1998]) to match the values of $\omega_{o,\text{meas},450}$ and $\omega_{o,\text{meas},700}$ at every altitude for every vertical profile. The linear combination method implies an externally mixed aerosol [Ackerman and Toon, 1981; Chylek et al., 1988; Jacobson, 2001; Chung and Seinfeld, 2005], but the goal in this step is to find a relationship that provides a constraint on the retrieval rather than a specific value. For the six vertical profiles, the average percentage of soot required to match $\omega_{o,\text{meas},450}$ and $\omega_{o,\text{meas},700}$ in the artificial

external mixture of soot and continental particles is 18% (standard deviation of 3%). For comparison, Bush and Valero [2002] showed that the polluted aerosol in India could be simulated with an external mixture of 81% sulfate and 19% soot ($\sim 3\%$ uncertainty) from d’Almeida et al. [1991] and if a sulfate and soot combination was used to simulate the SAFARI-2000 aerosol, 22% soot would be required (standard deviation of 3%).

[31] The values of $\omega_{o,\lambda}$ derived from linear combinations of soot with the different aerosol types given by d’Almeida et al. [1991] are shown in Figure 3 along with $\omega_{o,\lambda}$ from a model of Brazilian biomass burning aerosol [Ross et al., 1998] and $\omega_{o,\lambda}$ derived from methods applied to SAFARI-2000 data [Bergstrom et al., 2003]. The black circles are the column-averaged values of $\omega_{o,\lambda}$ at $\lambda = 450, 550,$ and 700 nm (based on the 3 λ -nephelometer and PSAP), while the solid black lines indicate the column-averaged uncertainty in $\omega_{o,\lambda}$ at $\lambda = 450, 550,$ and 700 nm. The soot contribution for each curve is adjusted to match values of $\omega_{o,450}$ and $\omega_{o,700}$ extrapolated from $\omega_{o,550}$. The potential range of possible values of $\omega_{o,\lambda}$ increases as a function of λ , and the soot and continental aerosol model is qualitatively in the middle of the range. To account for this increasing uncertainty, we apply about $\pm 10\%$ bounds to constrain the retrieval of $\omega_{o,\text{calc},\lambda}$ (equation (12)) for $\lambda < 450$ nm and $\lambda > 700$ nm. For comparison, the uncertainty in $\omega_{o,\lambda}$ measured at $\lambda = 550$ nm or extrapolated to other visible wavelengths is ± 3 – 6% .

4. Analysis

[32] The column-averaged, extinction-weighted mean values of the optically equivalent size distributions from each of the six profiles are listed in Table 2. The lognormal distributions that best reproduce the measured optical properties range from $D_g = 0.15$ – 0.22 μm (average of 0.19 ± 0.02 μm), with σ_g ranging from 1.7 to 1.9 (average of 1.8 ± 0.1). The values of N_a for the optically equivalent size distributions range from 1500 to 4600 cm^{-3} (average of 3600 ± 1300 cm^{-3}) for primarily submicron diameter particles (i.e., $D_g < 1$ μm). The values retrieved here agree with measurements of biomass burning aerosol size distributions from regions around the world and summarized by Reid et al. [2005a], who show that D_g ranges from 0.12 to 0.23 μm (mean is ~ 0.18 μm), while σ_g ranges from 1.3 to 1.8 (mean is ~ 1.6). The larger values of σ_g retrieved in this study are most likely due to the consideration of very small

particles and the assumption of a unimodal lognormal distribution.

[33] *Haywood et al.* [2003a] suggested a trimodal lognormal function to fit data collected during SAFARI-2000, but similar to the assumption in this study, the smallest mode ($D_g = 0.24 \pm 0.02 \mu\text{m}$, $\sigma_g = 1.3 \pm 0.1$, and $N_a = 1400 \pm 700 \text{ cm}^{-3}$) dominated the size distribution for transported biomass burning aerosol over Namibia, accounting for greater than 99% of N_a . The differences in the width (σ_g) are most likely due to the choice to model the biomass burning aerosol as a unimodal versus trimodal lognormal function, while the differences in N_a and D_g are due to the fact that N_a in this study includes smaller particles ($D_p = 0.01 \mu\text{m}$), whereas *Haywood et al.* [2003a] consider a size distribution starting at $D_p = 0.1 \mu\text{m}$. Of interest in this comparison is the fact that particle sizing instruments such as the PCASP-100x used in SAFARI-2000 on the UW research aircraft [*Magi, 2006*] and by the United Kingdom Met Office [*Haywood et al., 2003b; Osborne et al., 2004*] report values of extinction calculated from the PCASP measurements that are significantly less than the values of extinction derived from the nephelometer and PSAP.

[34] The ground-based photometers in the Aerosol Robotic Network (AERONET) described by *Holben et al.* [1998, 2001] retrieved size distributions ($D_p = 0.1\text{--}30 \mu\text{m}$) at a number of locations during SAFARI-2000 [*Eck et al., 2003*]. All AERONET data used in this study are using Version 2, Level 2.0 (cloud-screened, quality-controlled) data products (see <http://aeronet.gsfc.nasa.gov>). In a separate SAFARI-2000 study, *Leahy et al.* [2007] describe five UW vertical profiles that were discussed by *Magi et al.* [2003] which were within ~ 19 km of the AERONET ground sites and obtained within ~ 1 to 4 h of the AERONET retrieval times. In this study, we discuss three of the five profiles from *Leahy et al.* [2007] (labeled as ID = 1, 4, and 5 in Tables 2 and 3); these three profiles were within ~ 18 km of the AERONET ground sites and obtained within ~ 2 h of the AERONET retrievals. The effective diameters of the fine mode ($D_p < 1.2 \mu\text{m}$) size distributions from AERONET retrievals ranged from 0.26 to 0.29 μm , which once converted to D_g , are about the same as the values of D_g retrieved in this study.

[35] The column-averaged, extinction-weighted mean values of the wavelength-dependent, optically equivalent refractive indices for the UW vertical profiles are listed in Table 3. *Haywood et al.* [2003a, 2003b] suggested $m_{550} = 1.54 - 0.018i$ for biomass burning aerosol transported from east to west across southern Africa while the average (\pm standard deviation) in Table 3 is $m_{550} = (1.60 \pm 0.06) - (0.029 \pm 0.007)i$ for biomass burning aerosol closer to the sources. The higher values of $m_{i,\lambda}$ from the retrieval here compared to those for a more aged aerosol described by *Haywood et al.* [2003a, 2003b] are consistent with the thinking that aging processes result in a more scattering aerosol [*Reid et al., 2005a*].

[36] Values of retrieved $m_{i,\lambda}$ are higher for the September profiles than for the August profiles. When heavy tropical African biomass burning smoke was transported over the SAFARI-2000 sample region during a period from about 2 to 10 September 2000 called the ‘‘River of Smoke’’ [*Annegarn et al., 2002; Swap et al., 2003*], this resulted in higher values of $m_{i,\lambda}$ than when the SAFARI-2000 sample region was dominated by smoke from local sources [*Stein et al., 2003*].

Gao et al. [2003] and *Kirchstetter et al.* [2003] showed that the carbonaceous aerosol contribution to the overall aerosol composition increased during the River of Smoke. Referring to in situ measurements, this change during the River of Smoke corresponded to a decrease in $\omega_{o,\lambda}$, while an increase in N_a [*Magi, 2006*] resulted in an increase in τ_λ [*Magi et al., 2003*]. Thus the higher retrieved values of $m_{i,\lambda}$ during the River of Smoke profiles (September) is expected considering the strong contribution of absorption to the magnitude of $m_{i,\lambda}$ [*Bond and Bergstrom, 2006*].

[37] AERONET retrieved complex refractive index at $\lambda = 438, 669, 871, \text{ and } 1022 \text{ nm}$ based on sky radiance measurements [*Dubovik et al., 2000*]. In Figure 4, we show the comparison of m_λ retrieved using the methodology in this study and those reported by AERONET [*Eck et al., 2003*], showing only the three vertical profiles (discussed above) when the UW aircraft was colocated spatially and temporally with AERONET [*Leahy et al., 2007*]. There is no clear systematic bias in the overall wavelength dependence, but on average, $m_{r,\lambda}$ from AERONET during SAFARI-2000 is $\sim 14\%$ less than $m_{r,\lambda}$ in Table 3, while $m_{i,\lambda}$ from AERONET is $\sim 50\%$ less than $m_{i,\lambda}$ in Table 3. The differences in the wavelength dependence shown in Figure 4 are most likely due to the particle sizes considered in the individual retrievals; m_λ from AERONET is for particles with $D_p = 0.1\text{--}30 \mu\text{m}$, while m_λ in this study is for $D_p \sim 0.01\text{--}1 \mu\text{m}$ ($D_g = 0.06\text{--}0.985 \mu\text{m}$ in Table 1, but this refers to the mean diameter). Under high aerosol loading ($\tau_{440} > 0.5$), the estimated uncertainties in the absorption products from AERONET retrievals are low [*Dubovik et al., 2002*], but this study supports the ideas presented by *Ackerman et al.* [2004] and *Kahn et al.* [2004] that specific campaigns to characterize aerosol properties above AERONET sites [*Haywood et al., 2003a; Magi et al., 2005; Leahy et al., 2007; Schmid et al., 2006*] are needed to properly validate AERONET retrieved products. This is especially important since AERONET retrieved products are subsequently used to evaluate satellite products and model output [*Reddy et al., 2005; Zhou et al., 2005; Kinne et al., 2006; Ginoux et al., 2006*].

[38] The wavelength-dependent optical properties calculated from the optically equivalent size distributions and refractive indices are also listed in Table 3. After we apply the retrieval methodology to the data in Figure 2, we compare $\psi_{\text{meas},\lambda,z}$ to $\psi_{\text{calc},\lambda,z}$ (which are determined by $\phi_{\text{oe},\lambda,z}$) to assess the quality of the retrieval with respect to the original data at $\lambda = 450, 550, \text{ and } 700 \text{ nm}$. In Figure 5, we show the histogram distributions of the percent difference of the elements of $\psi_{\text{meas},\lambda,z}$ from the elements of $\psi_{\text{calc},\lambda,z}$, calculated as $100 * (\psi_{\text{calc},\lambda,z} - \psi_{\text{meas},\lambda,z}) / \psi_{\text{meas},\lambda,z}$ and sorted into evenly spaced bins. Data from $\lambda = 450, 550, \text{ and } 700 \text{ nm}$ and all altitudes are considered together in the histograms for a total of 417 points of comparison. A value of 1% in Figure 5 means that, for example, $\omega_{o,\text{calc},\lambda,z}$ calculated from the optically equivalent size distribution and refractive index (at λ) was 1% different from $\omega_{o,\text{meas},\lambda,z}$.

[39] In general, the elements of $\psi_{\text{calc},\lambda,z}$ vary by less than the typical uncertainties in the measured elements specified as $\delta_{\text{meas},\lambda,z}$ ($\pm 10\text{--}20\%$ for $\sigma_{\text{ext},\text{meas},\lambda,z}$, $\pm 3\text{--}6\%$ for $\omega_{o,\text{meas},\lambda,z}$, and $\pm 6\text{--}10\%$ for $\beta_{\text{meas},\lambda,z}$), which implies that the measured aerosol optical properties can be represented by the retrieved optically equivalent size distribution and

Table 3. Column-Averaged, Extinction-Weighted Mean Values of the Real (m_r) and Imaginary (m_i) Parts of the Optically Equivalent Refractive Index (m_{oe}) as a Function of Wavelength (λ) for the Six Vertical Profiles That Can Be Cross-Referenced Using the Numerical Identification (ID) in Table 2^a

λ , nm	m_{oe}		Calculated Optical Properties			
	m_r	m_i	σ_{ext} , Mm^{-1}	ω_o	g	β
<i>ID 1: 22 Aug 2000</i>						
354	1.55 ± 0.01	0.013 ± 0.002	190 ± 114	0.930 ± 0.008	0.649 ± 0.007	0.076 ± 0.002
380	1.53 ± 0.01	0.012 ± 0.002	168 ± 98	0.930 ± 0.009	0.648 ± 0.006	0.076 ± 0.002
449	1.54 ± 0.02	0.013 ± 0.002	133 ± 76	0.928 ± 0.010	0.626 ± 0.009	0.084 ± 0.003
450	1.52 ± 0.02	0.012 ± 0.002	125 ± 69	0.928 ± 0.010	0.628 ± 0.007	0.083 ± 0.002
499	1.56 ± 0.02	0.015 ± 0.002	108 ± 58	0.917 ± 0.010	0.598 ± 0.008	0.094 ± 0.003
525	1.59 ± 0.02	0.016 ± 0.002	98 ± 53	0.912 ± 0.011	0.578 ± 0.009	0.101 ± 0.003
550	1.59 ± 0.03	0.016 ± 0.003	86 ± 46	0.910 ± 0.012	0.567 ± 0.010	0.105 ± 0.003
606	1.63 ± 0.04	0.019 ± 0.003	73 ± 38	0.896 ± 0.012	0.537 ± 0.012	0.117 ± 0.004
675	1.68 ± 0.05	0.022 ± 0.003	57 ± 30	0.883 ± 0.014	0.496 ± 0.011	0.134 ± 0.004
700	1.74 ± 0.05	0.024 ± 0.003	55 ± 27	0.877 ± 0.014	0.484 ± 0.011	0.139 ± 0.004
778	1.77 ± 0.07	0.027 ± 0.004	46 ± 28	0.860 ± 0.016	0.451 ± 0.014	0.154 ± 0.006
865	1.78 ± 0.06	0.027 ± 0.004	38 ± 24	0.854 ± 0.017	0.436 ± 0.015	0.161 ± 0.006
1019	1.76 ± 0.07	0.029 ± 0.004	27 ± 14	0.828 ± 0.015	0.414 ± 0.014	0.170 ± 0.006
1241	1.79 ± 0.06	0.035 ± 0.005	21 ± 12	0.785 ± 0.015	0.388 ± 0.014	0.182 ± 0.006
1557	1.83 ± 0.07	0.049 ± 0.008	14 ± 9	0.693 ± 0.014	0.354 ± 0.017	0.198 ± 0.008
<i>ID 2: 24 Aug 2000</i>						
354	1.54 ± 0.02	0.021 ± 0.002	113 ± 157	0.890 ± 0.008	0.657 ± 0.017	0.074 ± 0.005
380	1.53 ± 0.02	0.021 ± 0.002	105 ± 140	0.891 ± 0.008	0.655 ± 0.017	0.074 ± 0.005
449	1.52 ± 0.02	0.022 ± 0.002	85 ± 120	0.881 ± 0.009	0.640 ± 0.022	0.079 ± 0.007
450	1.51 ± 0.02	0.022 ± 0.003	81 ± 113	0.880 ± 0.011	0.639 ± 0.021	0.079 ± 0.006
499	1.54 ± 0.02	0.025 ± 0.003	74 ± 106	0.869 ± 0.010	0.620 ± 0.021	0.086 ± 0.007
525	1.54 ± 0.02	0.026 ± 0.003	67 ± 97	0.865 ± 0.010	0.606 ± 0.022	0.091 ± 0.007
550	1.54 ± 0.02	0.026 ± 0.003	61 ± 88	0.858 ± 0.010	0.600 ± 0.023	0.093 ± 0.008
606	1.56 ± 0.02	0.029 ± 0.003	53 ± 80	0.845 ± 0.010	0.576 ± 0.025	0.103 ± 0.009
675	1.58 ± 0.03	0.032 ± 0.003	44 ± 69	0.827 ± 0.011	0.552 ± 0.031	0.112 ± 0.012
700	1.60 ± 0.04	0.034 ± 0.004	43 ± 67	0.823 ± 0.011	0.543 ± 0.033	0.117 ± 0.013
778	1.64 ± 0.05	0.040 ± 0.005	37 ± 62	0.800 ± 0.012	0.518 ± 0.037	0.127 ± 0.015
865	1.64 ± 0.04	0.039 ± 0.004	31 ± 53	0.792 ± 0.012	0.506 ± 0.038	0.133 ± 0.015
1019	1.62 ± 0.05	0.040 ± 0.005	26 ± 49	0.772 ± 0.011	0.506 ± 0.039	0.133 ± 0.016
1241	1.65 ± 0.06	0.050 ± 0.006	22 ± 48	0.729 ± 0.011	0.494 ± 0.039	0.139 ± 0.016
1557	1.71 ± 0.06	0.073 ± 0.010	18 ± 44	0.651 ± 0.011	0.469 ± 0.039	0.150 ± 0.017
<i>ID 3: 31 Aug 2000</i>						
354	1.59 ± 0.03	0.022 ± 0.003	148 ± 101	0.891 ± 0.011	0.589 ± 0.004	0.096 ± 0.002
380	1.57 ± 0.03	0.022 ± 0.003	136 ± 92	0.889 ± 0.013	0.587 ± 0.007	0.097 ± 0.003
449	1.58 ± 0.04	0.021 ± 0.003	97 ± 66	0.885 ± 0.014	0.553 ± 0.008	0.110 ± 0.003
450	1.59 ± 0.04	0.021 ± 0.003	97 ± 66	0.885 ± 0.013	0.552 ± 0.005	0.110 ± 0.002
499	1.63 ± 0.04	0.025 ± 0.003	80 ± 51	0.865 ± 0.015	0.511 ± 0.010	0.127 ± 0.004
525	1.65 ± 0.04	0.026 ± 0.003	74 ± 51	0.858 ± 0.014	0.496 ± 0.010	0.133 ± 0.004
550	1.70 ± 0.05	0.030 ± 0.004	67 ± 43	0.848 ± 0.015	0.481 ± 0.010	0.140 ± 0.004
606	1.70 ± 0.05	0.030 ± 0.004	57 ± 38	0.836 ± 0.019	0.454 ± 0.012	0.152 ± 0.005
675	1.78 ± 0.08	0.035 ± 0.005	45 ± 32	0.812 ± 0.018	0.414 ± 0.009	0.169 ± 0.004
700	1.82 ± 0.06	0.038 ± 0.005	42 ± 28	0.808 ± 0.018	0.406 ± 0.009	0.173 ± 0.004
778	1.84 ± 0.08	0.039 ± 0.005	30 ± 23	0.775 ± 0.021	0.358 ± 0.013	0.195 ± 0.006
865	1.82 ± 0.06	0.037 ± 0.005	25 ± 18	0.769 ± 0.021	0.353 ± 0.010	0.198 ± 0.005
1019	1.86 ± 0.08	0.038 ± 0.005	19 ± 13	0.744 ± 0.019	0.328 ± 0.014	0.209 ± 0.006
1241	1.86 ± 0.05	0.037 ± 0.004	14 ± 9	0.703 ± 0.020	0.295 ± 0.008	0.225 ± 0.004
1557	1.90 ± 0.06	0.042 ± 0.005	10 ± 7	0.620 ± 0.019	0.256 ± 0.014	0.244 ± 0.007
<i>ID 4: 3 Sep 2000</i>						
354	1.60 ± 0.02	0.035 ± 0.002	385 ± 302	0.848 ± 0.006	0.623 ± 0.004	0.084 ± 0.001
380	1.60 ± 0.02	0.035 ± 0.002	361 ± 318	0.847 ± 0.006	0.618 ± 0.003	0.086 ± 0.001
449	1.59 ± 0.02	0.036 ± 0.003	267 ± 201	0.836 ± 0.008	0.593 ± 0.004	0.094 ± 0.001
450	1.58 ± 0.02	0.035 ± 0.003	265 ± 206	0.836 ± 0.008	0.593 ± 0.004	0.094 ± 0.001
499	1.62 ± 0.02	0.037 ± 0.003	231 ± 190	0.834 ± 0.009	0.560 ± 0.005	0.106 ± 0.001
525	1.64 ± 0.03	0.037 ± 0.003	212 ± 162	0.834 ± 0.008	0.542 ± 0.004	0.113 ± 0.002
550	1.68 ± 0.03	0.038 ± 0.003	190 ± 141	0.831 ± 0.007	0.528 ± 0.004	0.120 ± 0.001
606	1.69 ± 0.04	0.038 ± 0.004	160 ± 127	0.826 ± 0.007	0.497 ± 0.005	0.132 ± 0.002
675	1.73 ± 0.05	0.038 ± 0.004	126 ± 110	0.823 ± 0.009	0.457 ± 0.007	0.149 ± 0.003
700	1.79 ± 0.06	0.041 ± 0.005	117 ± 95	0.820 ± 0.008	0.443 ± 0.006	0.156 ± 0.002
778	1.80 ± 0.06	0.044 ± 0.005	88 ± 78	0.792 ± 0.009	0.399 ± 0.008	0.175 ± 0.003
865	1.79 ± 0.05	0.042 ± 0.005	70 ± 63	0.784 ± 0.008	0.386 ± 0.010	0.182 ± 0.004
1019	1.76 ± 0.07	0.040 ± 0.006	50 ± 53	0.760 ± 0.007	0.369 ± 0.010	0.190 ± 0.004
1241	1.77 ± 0.07	0.043 ± 0.007	33 ± 43	0.719 ± 0.010	0.338 ± 0.009	0.205 ± 0.004
1557	1.81 ± 0.06	0.051 ± 0.007	22 ± 34	0.636 ± 0.008	0.295 ± 0.008	0.225 ± 0.004

Table 3. (continued)

λ , nm	m_{oe}		Calculated Optical Properties			
	m_r	m_i	σ_{ext} , Mm ⁻¹	ω_o	g	β
<i>ID 5: 6 Sep 2000</i>						
354	1.59 ± 0.01	0.033 ± 0.002	458 ± 171	0.850 ± 0.006	0.643 ± 0.007	0.079 ± 0.002
380	1.58 ± 0.01	0.033 ± 0.002	428 ± 184	0.848 ± 0.007	0.639 ± 0.007	0.080 ± 0.002
449	1.58 ± 0.02	0.036 ± 0.002	342 ± 138	0.835 ± 0.007	0.620 ± 0.008	0.086 ± 0.002
450	1.58 ± 0.02	0.036 ± 0.002	337 ± 146	0.834 ± 0.008	0.620 ± 0.008	0.086 ± 0.003
499	1.61 ± 0.02	0.037 ± 0.002	299 ± 148	0.835 ± 0.006	0.595 ± 0.011	0.095 ± 0.004
525	1.62 ± 0.03	0.037 ± 0.002	267 ± 111	0.833 ± 0.006	0.582 ± 0.013	0.100 ± 0.005
550	1.61 ± 0.03	0.036 ± 0.002	240 ± 96	0.832 ± 0.007	0.572 ± 0.013	0.103 ± 0.005
606	1.65 ± 0.03	0.037 ± 0.003	212 ± 103	0.832 ± 0.008	0.546 ± 0.014	0.114 ± 0.005
675	1.70 ± 0.04	0.038 ± 0.003	167 ± 71	0.830 ± 0.008	0.505 ± 0.017	0.130 ± 0.007
700	1.76 ± 0.06	0.041 ± 0.004	154 ± 66	0.824 ± 0.008	0.495 ± 0.016	0.135 ± 0.007
778	1.77 ± 0.06	0.045 ± 0.005	122 ± 60	0.801 ± 0.010	0.457 ± 0.018	0.150 ± 0.008
865	1.76 ± 0.06	0.043 ± 0.005	99 ± 50	0.794 ± 0.009	0.444 ± 0.019	0.156 ± 0.008
1019	1.70 ± 0.06	0.038 ± 0.006	64 ± 29	0.776 ± 0.010	0.424 ± 0.018	0.165 ± 0.008
1241	1.68 ± 0.08	0.039 ± 0.007	43 ± 17	0.730 ± 0.009	0.400 ± 0.021	0.177 ± 0.010
1557	1.68 ± 0.08	0.046 ± 0.008	29 ± 24	0.646 ± 0.009	0.361 ± 0.018	0.195 ± 0.008
<i>ID 6: 6 Sep 2000</i>						
354	1.57 ± 0.01	0.032 ± 0.002	421 ± 124	0.850 ± 0.007	0.653 ± 0.004	0.076 ± 0.001
380	1.57 ± 0.01	0.031 ± 0.002	399 ± 114	0.849 ± 0.007	0.649 ± 0.005	0.077 ± 0.001
449	1.57 ± 0.02	0.035 ± 0.002	317 ± 102	0.837 ± 0.008	0.629 ± 0.006	0.083 ± 0.002
450	1.57 ± 0.02	0.034 ± 0.002	309 ± 99	0.837 ± 0.008	0.631 ± 0.005	0.082 ± 0.001
499	1.59 ± 0.02	0.035 ± 0.002	272 ± 88	0.835 ± 0.008	0.610 ± 0.009	0.090 ± 0.003
525	1.59 ± 0.02	0.035 ± 0.002	245 ± 72	0.836 ± 0.008	0.598 ± 0.009	0.094 ± 0.003
550	1.59 ± 0.03	0.034 ± 0.002	222 ± 74	0.836 ± 0.009	0.590 ± 0.009	0.097 ± 0.003
606	1.62 ± 0.03	0.035 ± 0.003	198 ± 71	0.836 ± 0.009	0.567 ± 0.011	0.106 ± 0.004
675	1.65 ± 0.04	0.035 ± 0.003	156 ± 63	0.832 ± 0.009	0.532 ± 0.011	0.120 ± 0.004
700	1.70 ± 0.04	0.037 ± 0.004	142 ± 50	0.831 ± 0.010	0.519 ± 0.011	0.125 ± 0.005
778	1.72 ± 0.05	0.041 ± 0.004	114 ± 42	0.807 ± 0.010	0.483 ± 0.013	0.140 ± 0.005
865	1.69 ± 0.05	0.038 ± 0.005	91 ± 37	0.801 ± 0.010	0.475 ± 0.013	0.143 ± 0.006
1019	1.64 ± 0.06	0.035 ± 0.005	62 ± 21	0.782 ± 0.010	0.457 ± 0.014	0.151 ± 0.006
1241	1.61 ± 0.06	0.034 ± 0.006	40 ± 13	0.742 ± 0.009	0.427 ± 0.014	0.165 ± 0.006
1557	1.60 ± 0.07	0.040 ± 0.008	26 ± 9	0.656 ± 0.010	0.390 ± 0.016	0.182 ± 0.007

^aAlso listed are the column-averaged extinction coefficient (σ_{ext}), and the column-averaged, extinction-weighted single scattering albedo (ω_o), asymmetry parameter (g), and backscatter ratio (β) calculated using m_{oe} and the optically equivalent size distributions in Table 2. The values are listed as mean or weighted mean \pm 2 standard deviations. The column-averaged, scattering-weighted g is only a small fraction different than the column-averaged, extinction-weighted g shown in this table.

refractive indices to within measurement uncertainties. This agreement exists in part because the biomass burning aerosol in southern Africa is composed primarily of submicron diameter particles [Haywood *et al.*, 2003a; Eck *et al.*, 2003] that evolve to nearly spherical shapes [Posfai *et al.*, 2003] within hours after emission from the fires [Li *et al.*, 2003; Magi and Hobbs, 2003]. The bimodal percent difference distribution in Figure 5 for $\sigma_{ext,\lambda,z}$ arises from the generally larger percentage uncertainties associated with $\sigma_{ext,meas,\lambda,z}$ ($\delta\sigma_{ext,meas,\lambda,z}$) which weights the retrieval more heavily to values of $\omega_{o,meas,\lambda,z}$ and $\beta_{meas,\lambda,z}$ by equation (9).

[40] Values of $g_{\lambda,z}$ are not measured and are strictly a product of the retrieval, but we compare the results of the retrieval in this study with AERONET retrieved g_λ for the three cases discussed above. Values of g_λ retrieved by AERONET (for fine mode aerosol, $D_p < 1.2 \mu\text{m}$) are greater than g_λ retrieved in this study for $\lambda = 438 \text{ nm}$ and 669 nm but less than g_λ retrieved in this study for $\lambda = 871 \text{ nm}$ and 1022 nm . On average, g_λ retrieved by AERONET are (3 ± 11)% less than g_λ retrieved in this study and the difference ranges from -25% to $+7\%$. Thus the bias between the two retrievals is not systematic.

5. Summary

[41] We designed an original and straightforward retrieval algorithm that searches look-up tables constructed using

Mie theory to find a size distribution and refractive indices that most closely reproduce in situ and remote sensing measurements of aerosol optical properties. The optically equivalent size distribution and refractive indices are not necessarily representative of the real aerosol size distribution and refractive indices, especially if the aerosol is not composed of spherical particles, but they offer some insight into what properties are needed to reproduce available optical measurements.

[42] To properly constrain the retrieval, information about $\sigma_{ext,\lambda}$, $\omega_{o,\lambda}$, and β_λ are needed at least at three wavelengths. This is widely available for $\sigma_{sca,\lambda}$ and β_λ from nephelometry [Anderson *et al.*, 1996; Anderson and Ogren, 1998], and multiwavelength measurements of $\sigma_{abs,\lambda}$ are becoming more common [Ganguly *et al.*, 2005; Sheridan *et al.*, 2005; Virkkula *et al.*, 2005; Roden *et al.*, 2006; Schmid *et al.*, 2006]. The result is that $\sigma_{ext,\lambda}$ and $\omega_{o,\lambda}$ at three wavelength can be readily derived. For SAFARI-2000, $\sigma_{abs,\lambda}$ was only measured at one wavelength [Magi *et al.*, 2003] and we extrapolated this to two other wavelengths using other data collected during SAFARI-2000 and described by Bergstrom *et al.* [2003]. This reduces the number of constraints on the retrieval from nine to eight, such that we have eight knowns and nine unknowns. To account for this underdetermined problem, we use SAFARI-2000 measurements of N_a as an additional constraint on the retrieval. The resolution of the

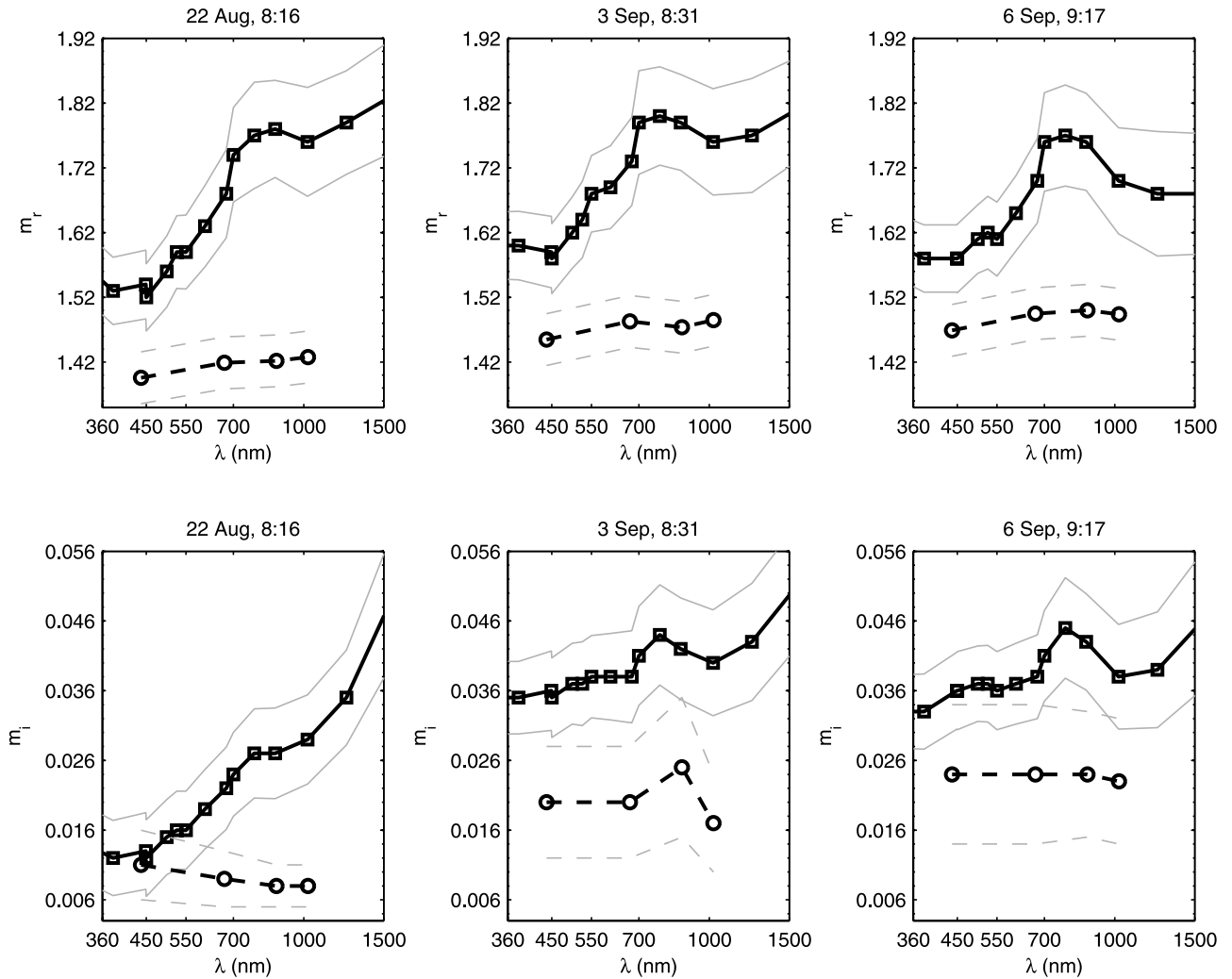


Figure 4. Comparison of the real and imaginary refractive indices (m_r and m_i , respectively) as functions of wavelength (λ) derived from the retrieval in this study (line with squares) and reported by AERONET (dashed line with circles). The titles list the dates (year 2000) and UTC times of the three UW research aircraft vertical profiles (corresponding to ID = 1, 4, and 5 in Table 2) which were obtained within ~ 18 km of AERONET stations and within ~ 2 h of the AERONET retrievals. The squares and circles denote the specific wavelengths of the individual retrievals. The confidence limits in m_r and m_i from the retrieval in this study (solid thin shaded lines) are determined from variability within a vertical profile (listed in Table 3) and uncertainty in retrieval itself (± 0.05 for m_r and ± 0.005 for m_i , per Table 1). The confidence limits in the AERONET retrieved values (dashed thin shaded lines) are ± 0.04 for m_r and $\pm 40\%$ for m_i [Dubovik *et al.*, 2002].

look-up tables used in the retrieval is adequate to resolve the optical properties to within typical uncertainties (section 3.1), while the so-called structural uncertainties in calculated optical properties that arise from the discrete input used to build the look-up tables (Table 1) are $\pm 4.1\%$ for $\sigma_{\text{ext},\lambda}$, $\pm 1.2\%$ for $\omega_{o,\lambda}$, and $\pm 3.8\%$ for g_λ (section 2.4).

[43] From the more detailed and readily available measurements at three visible wavelengths, we retrieve the optically equivalent size distribution and refractive index and use this information with derived values of $\sigma_{\text{ext},\lambda}$ at $\lambda = 354\text{--}1557$ nm from the NASA Ames Airborne Tracking Sun photometer on the UW research aircraft [Schmid *et al.*, 2003] as the basis for a simple search algorithm to obtain self-consistent aerosol optical properties. However, with no

data available about $\omega_{o,\lambda}$ beyond $\lambda = 550$ nm during SAFARI-2000, we combine an assumption of α_{abs} for visible wavelengths based on two case studies from SAFARI-2000 [Bergstrom *et al.*, 2003; Pilewskie *et al.*, 2003] with the assumption of a continental and soot aerosol combination [d'Almeida *et al.*, 1991] to serve as a constraint on $\omega_{o,\lambda}$. If in future studies, a better understanding of the regional dependence of α_{abs} developed from, say, more detailed measurements [Ganguly *et al.*, 2005; Sheridan *et al.*, 2005; Virkkula *et al.*, 2005; Bond and Bergstrom, 2006; Roden *et al.*, 2006], this retrieval could easily be modified to utilize the information.

[44] Although the optically equivalent size distribution and bulk refractive index from the retrieval are not neces-

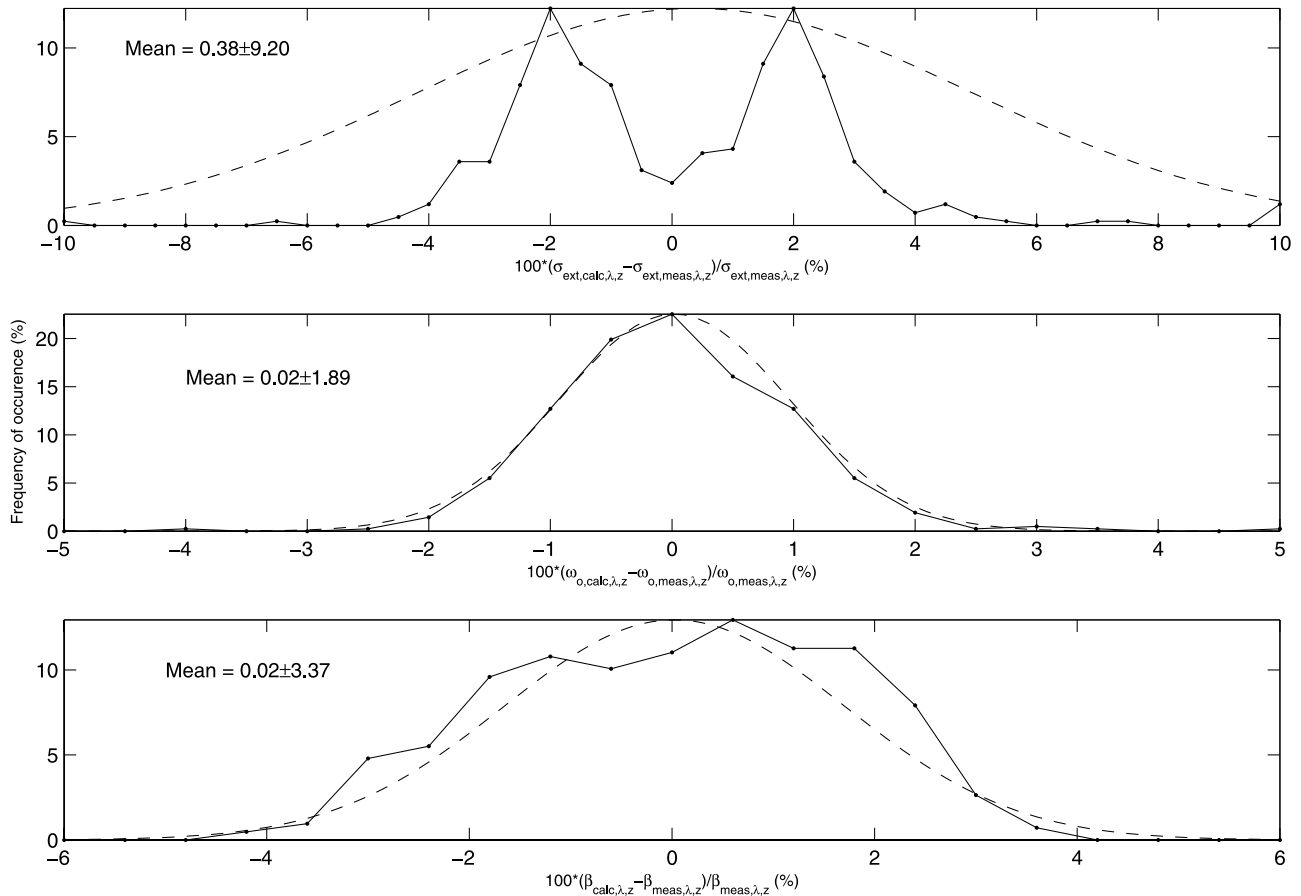


Figure 5. Histograms showing the average percent differences between measured optical properties and those calculated from the retrieved optically equivalent size distribution and refractive indices. Uncertainties in the measured optical properties are ± 10 – 20% for $\sigma_{\text{ext, meas, } \lambda, z}$, ± 3 – 6% for $\omega_{\text{o, meas, } \lambda, z}$, and ± 6 – 10% for $\beta_{\text{meas, } \lambda, z}$. The dashed curves are the Gaussian distribution functions given by the mean (± 2 standard deviations) in each figure. The solid curves connect the points that denote the center of the various bins. The number of points used to compile each of the histograms is 417.

sarily representative of the true size distribution and refractive index, we showed that the optically equivalent size distributions in Table 2 are similar to the submicron modes of the size distributions in the works of *Haywood et al.* [2003a, 2003b] and retrieved from AERONET [*Eck et al.*, 2003] during SAFARI-2000. The retrieval in this study reports higher values of N_a than *Haywood et al.* [2003a], but as discussed in section 4, we include smaller diameter particles. However, the optically equivalent real and imaginary refractive indices derived in this study (Table 3) are, respectively, $\sim 14\%$ and $\sim 50\%$ greater than those derived from AERONET retrievals for three cases when comparisons can be made, and in some cases show a very different wavelength dependence.

[45] In southern Africa, fluctuations in the aerosol properties of the regional haze during the biomass burning season are primarily due to fluctuations in the number of biomass fires [*Eck et al.*, 2003; *Magi et al.*, 2003], and the biomass burning aerosol is dominated by submicron diameter [*Haywood et al.*, 2003a; *Eck et al.*, 2003], nearly spherical [*Posfai et al.*, 2003] particles that age rapidly away from the fire source [*Li et al.*, 2003; *Magi and Hobbs*, 2003]. The retrieval presented here is thus particularly well

sued for SAFARI-2000 data since supermicron diameter, nonspherical particles play a minimal role in southern African aerosol optical properties. For locations where supermicron diameter particles, like mineral dust, play a more significant role, the retrieval methodology in this study would require information specific to the supermicron mode of the aerosol size distribution [e.g., *Clarke et al.*, 2002; *Doherty et al.*, 2005] to properly constrain the larger solution space. The retrieval would also require a different approach if the aerosol is composed of particles that cannot be represented with spheres.

[46] The results of the retrieval offer a method to find self-consistent aerosol properties such that closure between independent measurements can be obtained or, conversely, that potential discrepancies between in situ instruments [*Haywood et al.*, 2003b; *Osborne et al.*, 2004] are highlighted. Combining the retrieval methodology with the methodology presented by *Magi et al.* (submitted manuscript, 2007) provides a method to transition from field measurements to model input, assuming the measurements themselves properly characterize the regional aerosol. The retrieval methodology is constrained by data that has been routinely collected in other aerosol measurement campaigns

[Reid et al., 1998; Clarke et al., 2002; Russell et al., 2002; Doherty et al., 2005; Magi et al., 2005; Redemann et al., 2006; Schmid et al., 2006]. We urge the measurement community to apply the retrieval methodology described in this study whenever the required constraints are available. This would provide a good point for comparison with model input or with available climatologies of aerosol properties [d'Almeida et al., 1991; Hess et al., 1998]. If this retrieval is modified, data about supermicron diameter particles could be used and provide even more information.

[47] Most of the measurements made from the University of Washington (UW) research aircraft during SAFARI-2000 have not been incorporated into any model of southern African biomass burning [e.g., Abel et al., 2005; Kinne et al., 2006]. Magi et al. (submitted manuscript, 2007) describe a methodology to derive aerosol radiative forcing from in situ measurements by combining the retrieval methodology in this study with a radiative transfer model, while in future work, we discuss the broader implications of the measurement-based estimates of biomass burning aerosol radiative forcing using multiyear satellite data. In the end, combining the various methodologies with the data collected on the UW research aircraft during SAFARI-2000 can offer important comparisons with model input at a regional level as well as with ground-based and satellite-derived aerosol products.

[48] **Acknowledgments.** We thank the late Peter Hobbs for his support during the research phase of this project. We want to acknowledge the work of the science and the flight crews for the University of Washington research aircraft during the SAFARI-2000 field campaign. Valuable discussions with Dean Hegg, Tad Anderson, and Tom Ackerman, as well as comments by three anonymous reviewers, helped improve this research. We thank Brent Holben and Stuart Piketh for their efforts in establishing and maintaining the Mongu, Sua Pan, and Skukuza AERONET sites in southern Africa. B.M. is supported in part by NSF grant 0314453 and by NASA grant NNG04GM23G. Q.F. is in part supported by NASA grant NNG04GM23G.

References

- Abel, S. J., E. J. Highwood, J. M. Haywood, and M. A. Stringer (2005), The direct radiative effects of biomass burning aerosols over southern Africa, *Atmos. Chem. Phys.*, *5*, 1999–2018.
- Ackerman, T. P., and O. B. Toon (1981), Absorption of visible radiation in atmosphere containing mixtures of absorbing and non-absorbing particles, *Appl. Opt.*, *20*(20), 3661–3668.
- Ackerman, T. P., A. J. Braverman, D. J. Diner, T. L. Anderson, R. A. Kahn, J. V. Martonchik, J. E. Penner, P. J. Rasch, B. A. Wielicki, and B. Yu (2004), Integrating and interpreting aerosol observations and models within the PARAGON framework, *Bull. Am. Meteorol. Soc.*, *85*, 1523–1533.
- Anderson, T. L., and J. A. Ogren (1998), Determining aerosol radiative properties using the TSI 3563 integrating nephelometer, *Aerosol Sci. Technol.*, *29*, 57–69.
- Anderson, T. L., et al. (1996), Performance characteristics of a high-sensitivity, three-wavelength total scatter/backscatter nephelometer, *J. Atmos. Oceanic Technol.*, *13*, 967–986.
- Anderson, T. L., S. J. Masonis, D. S. Covert, R. J. Charlson, and M. J. Rood (2000), In situ measurement of the aerosol extinction-to-backscatter ratio at a polluted continental site, *J. Geophys. Res.*, *105*(D22), 26,907–26,915.
- Anderson, T. L., R. J. Charlson, S. E. Schwartz, R. Knutti, O. Boucher, H. Rodhe, and J. Heintzenberg (2003), Climate forcing by aerosols—A hazy picture, *Science*, *300*, 1103–1104.
- Andreae, M. O., C. D. Jones, and P. M. Cox (2005), Strong present-day aerosol cooling implies a hot future, *Nature*, *435*, 1187–1190.
- Annegarn, H. J., L. Otter, R. J. Swap, and R. J. Scholes (2002), Southern Africa's ecosystem in a test-tube, *S. Afr. J. Sci.*, *98*, 111–113.
- Bergstrom, R. W., P. Pilewskie, B. Schmid, and P. B. Russell (2003), Estimates of the spectral aerosol single scattering albedo and aerosol radiative effects during SAFARI 2000, *J. Geophys. Res.*, *108*(D13), 8474, doi:10.1029/2002JD002435.
- Bevington, P. R., and D. K. Robinson (1992), *Data Reduction and Error Analysis for the Physical Sciences*, 2nd ed., 328 pp., McGraw-Hill, New York.
- Bohren, C. F., and D. R. Huffman (1983), *Absorption and Scattering of Light by Small Particles*, 530 pp., John Wiley, Hoboken, N. J.
- Bond, T. C., and R. W. Bergstrom (2006), Light absorption by carbonaceous particles: An investigative review, *Aerosol Sci. Technol.*, *40*, 27–67.
- Bond, T. C., T. L. Anderson, and D. Campbell (1999), Calibration and intercomparison of filter-based measurements of visible light absorption by aerosols, *Aerosol Sci. Technol.*, *30*, 582–600.
- Bond, T. C., D. G. Streets, K. F. Yarber, S. M. Nelson, J. Woo, and Z. Klimont (2004), A technology-based global inventory of black and organic carbon emissions from combustion, *J. Geophys. Res.*, *109*, D14203, doi:10.1029/2003JD003697.
- Bush, B. C., and F. P. J. Valero (2002), Spectral aerosol radiative forcing at the surface during the Indian Ocean Experiment (INDOEX), *J. Geophys. Res.*, *107*(D19), 8003, doi:10.1029/2000JD000020.
- Chung, S. H., and J. H. Seinfeld (2005), Climate response of direct radiative forcing of anthropogenic black carbon, *J. Geophys. Res.*, *110*, D11102, doi:10.1029/2004JD005441.
- Chylek, P., V. Srivastava, R. G. Pinnick, and R. T. Wang (1988), Scattering of electromagnetic waves by composite spherical particles: Experiment and effective medium approximations, *Appl. Opt.*, *27*, 2396–2404.
- Clarke, A. D., et al. (2002), INDOEX aerosol: A comparison and summary of chemical microphysical, and optical properties observed from land, ship, and aircraft, *J. Geophys. Res.*, *107*(D19), 8033, doi:10.1029/2001JD000572.
- d'Almeida, G. A., P. Koepke, and E. P. Shettle (Eds.) (1991), *Atmospheric Aerosols: Global Climatology and Radiative Characteristics*, 561 pp., A. Deepak Publishing, Hampton, Va.
- Dave, J. V. (1970), Coefficients of the Legendre and Fourier series for the scattering functions of spherical particles, *Appl. Opt.*, *9*, 1888–1896.
- Delworth, T. L., V. Ramaswamy, and G. L. Stenchikov (2005), The impacts of aerosols on simulated ocean temperature and heat content in the 20th century, *Geophys. Res. Lett.*, *32*, L24709, doi:10.1029/2005GL024457.
- Doherty, S., P. K. Quinn, A. Jefferson, C. M. Carrico, T. L. Anderson, and D. Hegg (2005), A comparison and summary of aerosol optical properties as observed in situ from aircraft, ship, and land during ACE-Asia, *J. Geophys. Res.*, *110*, D04201, doi:10.1029/2004JD004964.
- Dubovik, O., A. Smirnov, B. N. Holben, M. D. King, Y. J. Kaufman, T. F. Eck, and I. Slutsker (2000), Accuracy assessments of aerosol optical properties retrieved from Aerosol Robotic Network (AERONET) Sun and sky radiance measurements, *J. Geophys. Res.*, *105*(D8), 9791–9806.
- Dubovik, O., B. Holben, T. F. Eck, A. Smirnov, Y. J. Kaufman, M. D. King, D. Tanre, and I. Slutsker (2002), Variability of absorption and optical properties of key aerosol types observed in worldwide locations, *J. Atmos. Sci.*, *59*, 590–608.
- Eck, T. F., et al. (2003), Variability of biomass burning aerosol optical characteristics in southern Africa during the SAFARI 2000 dry season campaign and a comparison of single scattering albedo estimates from radiometric measurements, *J. Geophys. Res.*, *108*(D13), 8477, doi:10.1029/2002JD002321.
- Ganguly, D., A. Jayaraman, H. Gadhavi, and T. A. Rajesh (2005), Features in wavelength dependence of aerosol absorption observed over central India, *Geophys. Res. Lett.*, *32*, L13821, doi:10.1029/2005GL023023.
- Gao, S., D. A. Hegg, P. V. Hobbs, T. W. Kirchstetter, B. I. Magi, and M. Sadilek (2003), Water-soluble organic components in aerosols associated with savanna fires in southern Africa: Identification, evolution, and distribution, *J. Geophys. Res.*, *108*(D13), 8491, doi:10.1029/2002JD002324.
- Genoux, P., L. W. Horowitz, V. Ramaswamy, I. V. Geogdzhayev, B. N. Holben, G. Stenchikov, and X. Tie (2006), Evaluation of aerosol distribution and optical depth in the Geophysical Fluid Dynamics Laboratory coupled model CM2.1 for present climate, *J. Geophys. Res.*, *111*, D22210, doi:10.1029/2005JD006707.
- Hansen, J., et al. (2005), Earth's energy imbalance: Confirmation and implications, *Science*, *308*, 1431–1435.
- Hartley, W. S. (2000), Airborne study of aerosol optical properties and direct aerosol radiative forcing off the east coast of the United States, M. S. thesis, 271 pp., Univ. of Washington, Seattle.
- Hartley, W. S., and P. V. Hobbs (2001), An aerosol model and aerosol-induced changes in the clear-sky albedo off the east coast of the United States, *J. Geophys. Res.*, *106*(D9), 9733–9748.
- Haywood, J. M., S. R. Osborne, P. N. Francis, A. Keil, P. Formenti, M. O. Andreae, and P. H. Kaye (2003a), The mean physical and optical properties of regional haze dominated biomass burning aerosol measured from the C-130 aircraft during SAFARI 2000, *J. Geophys. Res.*, *108*(D13), 8473, doi:10.1029/2002JD002226.
- Haywood, J., P. Francis, O. Dubovik, M. Glew, and B. Holben (2003b), Comparison of aerosol size distributions, radiative properties, and optical depths determined by aircraft observations and Sun photometers during

- SAFARI 2000, *J. Geophys. Res.*, *108*(D13), 8471, doi:10.1029/2002JD002250.
- Hess, M., P. Koepke, and I. Schult (1998), Optical Properties of Aerosols and Clouds: The software package OPAC, *Bull. Am. Meteorol. Soc.*, *79*(5), 831–844.
- Hobbs, P. V., P. Sinha, R. J. Yokelson, I. T. Bertschi, D. R. Blake, S. Gao, T. W. Kirchstetter, T. Novakov, and P. Pilewskie (2003), Evolution of gases and particles from a savanna fire in South Africa, *J. Geophys. Res.*, *108*(D13), 8485, doi:10.1029/2002JD002352.
- Holben, B. N., et al. (1998), AERONET—A federated instrument network and data archive for aerosol characterization, *Remote Sens. Environ.*, *66*, 1–16.
- Holben, B. N., et al. (2001), An emerging ground-based aerosol climatology: Aerosol optical depth from AERONET, *J. Geophys. Res.*, *106*(D11), 12,067–12,097.
- Jacobson, M. Z. (2001), Global direct radiative forcing due to multicomponent anthropogenic and natural aerosols, *J. Geophys. Res.*, *106*(D2), 1551–1568.
- Kahn, R. A., J. A. Ogren, T. P. Ackerman, J. Boesenberg, R. J. Charlson, D. J. Diner, B. N. Holben, R. T. Menzies, M. A. Miller, and J. H. Seinfeld (2004), Aerosol data sources and their roles within PARAGON, *Bull. Am. Meteorol. Soc.*, *85*, 1511–1522.
- Kinne, S., et al. (2006), An AeroCom initial assessment—Optical properties in aerosol component modules of global models, *Atmos. Chem. Phys.*, *6*, 1815–1834.
- Kirchstetter, T. W., T. Novakov, P. V. Hobbs, and B. Magi (2003), Airborne measurements of carbonaceous aerosols in southern Africa during the dry, biomass burning season, *J. Geophys. Res.*, *108*(D13), 8476, doi:10.1029/2002JD002171.
- Kirchstetter, T. W., T. Novakov, and P. V. Hobbs (2004), Evidence that the spectral dependence of light absorption by aerosols is affected by organic carbon, *J. Geophys. Res.*, *109*, D21208, doi:10.1029/2004JD004999.
- Leahy, L. V., T. L. Anderson, T. F. Eck, and R. W. Bergstrom (2007), A synthesis of single scattering albedo of biomass burning aerosol over southern Africa during SAFARI 2000, *Geophys. Res. Lett.*, *34*, L12814, doi:10.1029/2007GL029697.
- Li, J., M. Posfai, P. V. Hobbs, and P. R. Buseck (2003), Individual aerosol particles from biomass burning in southern Africa: 2. Compositions and aging of inorganic particles, *J. Geophys. Res.*, *108*(D13), 8484, doi:10.1029/2002JD002310.
- Magi, B. I. (2006), Optical properties and radiative forcing of southern African biomass burning aerosol, Ph. D. thesis, 180 pp., Univ. of Washington, Seattle.
- Magi, B. I., and P. V. Hobbs (2003), Effects of humidity on aerosols in southern Africa during the biomass burning season, *J. Geophys. Res.*, *108*(D13), 8495, doi:10.1029/2002JD002144.
- Magi, B. I., P. V. Hobbs, B. Schmid, and J. Redemann (2003), Vertical profiles of light scattering, light absorption and single-scattering albedo during the dry, biomass burning season in southern Africa and comparisons of in-situ and remote sensing measurements of aerosol optical depth, *J. Geophys. Res.*, *108*(D13), 8504, doi:10.1029/2002JD002361.
- Magi, B. I., P. V. Hobbs, T. W. Kirchstetter, T. Novakov, D. A. Hegg, S. Gao, J. Redemann, and B. Schmid (2005), Aerosol properties and chemical apportionment of aerosol optical depth at locations off the United States east coast in July and August 2001, *J. Atmos. Sci.*, *62*(4), 919–933.
- Osborne, S. R., J. M. Haywood, P. N. Francis, and O. Dubovik (2004), Short-wave radiative effects of biomass burning aerosol during SAFARI2000, *Q. J. R. Meteorol. Soc.*, *130*, 1423–1447.
- Pilewskie, P., J. Pommier, R. Bergstrom, W. Gore, S. Howard, M. Rabbette, B. Schmid, P. V. Hobbs, and S. C. Tsay (2003), Solar spectral radiative forcing during the Southern African Regional Science Initiative, *J. Geophys. Res.*, *108*(D13), 8486, doi:10.1029/2002JD002411.
- Posfai, M., R. Simonics, J. Li, P. V. Hobbs, and P. R. Buseck (2003), Individual aerosol particles from biomass burning in southern Africa: 1. Compositions and size distributions of carbonaceous particles, *J. Geophys. Res.*, *108*(D13), 8483, doi:10.1029/2002JD002291.
- Quinn, P. K., and T. S. Bates (2005), Regional aerosol properties: Comparisons from ACE 1, ACE 2, Aerosols99, INDOEX, ACE Asia, TARFOX, and NEAQS, *J. Geophys. Res.*, *110*, D14202, doi:10.1029/2004JD004755.
- Reddy, M. S., O. Boucher, N. Bellouin, M. Schulz, Y. Balkanski, J. L. Dufresne, and M. Pham (2005), Estimates of global multicomponent aerosol optical depth and direct radiative perturbation in the Laboratoire de Meteorologie-Dynamique general circulation model, *J. Geophys. Res.*, *110*, D10S16, doi:10.1029/2004JD004757.
- Redemann, J., et al. (2000), Retrieving the vertical structure of the effective aerosol complex index of refraction from a combination of aerosol in situ and remote sensing measurements during TARFOX, *J. Geophys. Res.*, *105*(D8), 9949–9970.
- Redemann, J., P. Pilewskie, P. B. Russell, J. M. Livingston, S. Howard, B. Schmid, J. Pommier, W. Gore, J. Eilers, and M. Wendisch (2006), Airborne measurements of spectral direct aerosol radiative forcing in the Intercontinental Chemical Transport Experiment/Intercontinental Transport and Chemical Transformation of anthropogenic pollution 2004, *J. Geophys. Res.*, *111*, D14210, doi:10.1029/2005JD006812.
- Reid, J. S., P. V. Hobbs, R. J. Ferek, D. R. Blake, J. V. Martins, M. R. Dunlap, and C. Liousse (1998), Physical, chemical and optical properties of regional hazes dominated by smoke in Brazil, *J. Geophys. Res.*, *103*(D24), 32,059–32,080.
- Reid, J. S., R. Koppmann, T. F. Eck, and D. P. Eleuterio (2005a), A review of biomass burning emissions. Part II: Intensive physical properties of biomass burning particles, *Atmos. Chem. Phys.*, *5*, 799–825.
- Reid, J. S., T. F. Eck, S. A. Christopher, R. Koppmann, O. Dubovik, D. P. Eleuterio, B. N. Holben, E. A. Reid, and J. Zhang (2005b), A review of biomass burning emissions. Part III: Intensive optical properties of biomass burning particles, *Atmos. Chem. Phys.*, *5*, 827–849.
- Roden, C. A., T. C. Bond, S. Conway, and A. B. O. Pinnel (2006), Emission factors and real-time optical properties of particles emitted from traditional wood burning cookstoves, *Environ. Sci. Technol.*, *40*, 6750–6757.
- Ross, J. L., P. V. Hobbs, and B. Holben (1998), Radiative characteristics of regional hazes dominated by smoke from biomass burning in Brazil: Closure tests and direct radiative forcing, *J. Geophys. Res.*, *103*(D24), 31,925–31,941.
- Russell, P. B., et al. (2002), Comparison of aerosol single scattering albedos derived by diverse techniques in two North Atlantic experiments, *J. Atmos. Sci.*, *59*, 609–619.
- Schmid, B., et al. (2003), Coordinated airborne, spaceborne, and ground-based measurements of massive, thick aerosol layers during the dry season in southern Africa, *J. Geophys. Res.*, *108*(D13), 8496, doi:10.1029/2002JD002297.
- Schmid, B., et al. (2006), How well do state-of-the-art techniques measuring the vertical profile of tropospheric aerosol extinction compare?, *J. Geophys. Res.*, *111*, D05S07, doi:10.1029/2005JD005837.
- Schwartz, S. E. (2004), Uncertainty requirements in radiative forcing of climate change, *J. Air Waste Manage. Assoc.*, *54*, 1351–1359.
- Seinfeld, J. H., and S. N. Pandis (1998), *Atmospheric Chemistry and Physics: From Air Pollution to Climate Change*, 1326 pp., John Wiley, Hoboken, N. J.
- Sheridan, P. J., et al. (2005), The Reno Aerosol Optics Study: An evaluation of aerosol absorption measurement methods, *Aerosol Sci. Technol.*, *29*, 1–16.
- Sinha, P., P. V. Hobbs, R. J. Yokelson, I. T. Bertschi, D. R. Blake, I. J. Simpson, S. Gao, T. W. Kirchstetter, and T. Novakov (2003), Emissions of trace gases and particles from savanna fires in southern Africa, *J. Geophys. Res.*, *108*(D13), 8487, doi:10.1029/2002JD002325.
- Stein, D. C., R. J. Swap, S. Greco, S. J. Piketh, S. A. Macko, B. G. Doddridge, T. Elias, and R. T. Bruinjes (2003), Haze layer characterization and associated meteorological controls along the eastern coastal region of southern Africa, *J. Geophys. Res.*, *108*(D13), 8506, doi:10.1029/2002JD003237.
- Swap, R. J., H. J. Annegarn, J. T. Suttles, M. D. King, S. Platnick, J. L. Privette, and R. J. Scholes (2003), Africa burning: A thematic analysis of the Southern African Regional Science Initiative (SAFARI 2000), *J. Geophys. Res.*, *108*(D13), 8465, doi:10.1029/2003JD003747.
- Virkkula, A., N. C. Ahlquist, D. S. Covert, W. P. Arnott, P. J. Sheridan, P. K. Quinn, and D. J. Coffman (2005), Modification, calibration and a field test of an instrument for measuring light absorption by particles, *Aerosol Sci. Technol.*, *36*, 68–83.
- Wiscombe, W. (1980), Improved Mie scattering algorithms, *Appl. Opt.*, *19*(9), 1505–1509.
- Zhou, M., H. Yu, R. E. Dickinson, O. Dubovik, and B. N. Holben (2005), A normalized description of the direct effect of key aerosol types on solar radiation as estimated from Aerosol Robotic Network aerosols and Moderate Resolution Imaging Spectroradiometer albedos, *J. Geophys. Res.*, *110*, D19202, doi:10.1029/2005JD005909.

Q. Fu and B. I. Magi, Department of Atmospheric Sciences, University of Washington, Seattle, WA 98195, USA. (magi@atmos.washington.edu)
J. Redemann, Bay Area Environmental Research Institute, Sonoma, CA 95476, USA.